BAMS Article

Super Drought under Global Warming

Concept, Monitoring Index, and Validation

Lin Wang, Gang Huang, Wen Chen, and Ting Wang

ABSTRACT: Recent decades have witnessed growing frequency and severity of catastrophic droughts in many regions of the world. Despite lots of studies having been dedicated to extreme drought investigation, the fundamental question that has long been ignored is, What is extreme drought? The answer is much more complex than it first appears, because a critical issue in the study of drought is the multiscalar nature. To address the challenge, this study establishes the theoretical basis of the super drought concept, which refers to the simultaneous occurrence of extreme droughts at multiple time scales. The physical significance of super drought represents compound dry extremes in all parts of water resources or equivalently a grand loss in total water storage, which is identified as the essential determinant distinguishing high-impact droughts from those causing mild damage. To have a quantitative representation, a novel monitoring index called comprehensive multiscalar index (CMI) is developed based on the vine copula framework. It turns out that CMI is a plausible measure to determine the overall rarity of multiscalar drought and recognize super drought. Furthermore, the worldwide skill of CMI and super drought identification are testified against Gravity Recovery and Climate Experiment (GRACE) total water storage. Compared to traditional indices that lack comprehensive treatment of drought, CMI performs better in capturing the variation of overall water availability and enables the accurate detection of real water scarcity, with gross improvements in correlation and root-mean-square error scores exceeding the 10^{-3} significance level. To facilitate end users and policy-makers, near-real-time monitoring and a historical data repository are available through the public website superdrought.com.

KEYWORDS: Drought; Extreme events; Water resources; Indices; Climate; Hydrology

https://doi.org/10.1175/BAMS-D-22-0182.1
Corresponding authors: Lin Wang, linwang@mail.iap.ac.cn and wang_lin@mail.iap.ac.cn; Gang Huang, hg@mail.iap.ac.cn
Supplemental material: https://doi.org/10.1175/BAMS-D-22-0182.2

In final form 26 February 2023

AFFILIATIONS: L. Wang—CAS Key Laboratory of Regional Climate-Environment for Temperate East Asia, Institute of Atmospheric Physics, Chinese Academy of Sciences, Beijing, China; **Huang**—State Key Laboratory of Numerical Modeling for Atmospheric Sciences and Geophysical Fluid Dynamics, Institute of Atmospheric Physics, Chinese Academy of Sciences, Beijing, China; **Chen**—Department of Atmospheric Science, Yunnan University, Kunming, China; **T. Wang**—Carbon Neutrality Research Center, Institute of Atmospheric Physics, Chinese Academy of Sciences, Beijing, China

Drought is one of the most damaging hazards worldwide, due to its prolonged and extensive impacts on agriculture, ecosystems, economy, and human society (Dai 2011; Ault 2020; AghaKouchak et al. 2021; Van Loon et al. 2016). In total, it is recorded that 1.4 billion people were affected by droughts in the period 2000–19 (UNDRR 2020). Under global warming, though the long-term trends in drought frequency and severity on a global scale remain an element of debate (Dai 2013; Sheffield et al. 2012; Huang et al. 2016; Berg and McColl 2021; Trenberth et al. 2014), drought conditions have unprecedentedly worsened in many regions of the world (Fu and Feng 2014; Sherwood and Fu 2014; He et al. 2020; Huang et al. 2017; Guan et al. 2019). The hotspots frequently struck by extreme drought events are southwestern North America (Williams et al. 2022), Southwest and southern China (Wang et al. 2015; Zhang et al. 2020; Wang et al. 2021), the transitional climate zone in East Asia (L. Wang et al. 2022), Europe (Naumann et al. 2021), the Amazonia (Lewis et al. 2011), Africa (Pascale et al. 2020), and Australia (Peterson et al. 2021). Future projection highlights significant drying tendency in most of the Americas, the Mediterranean region, southern Africa, and Australia (Zhao and Dai 2017, 2022; Qi et al. 2022; Spinoni et al. 2020). Recently, the United Nations warned that we are standing at a crossroads, as land is drying up, fertile grounds are turning to dust, and drought is prevailing (UNCCD 2022).

Facing the growing frequency of extreme drought events globally, much effort has been expended on the exploration and explanation of this area (J. Wang et al. 2022). However, the fundamental question that has long been ignored is, What is the extreme status of drought? It seems simple, as the event is typically defined as extreme if the observed value is above or below a certain percentile (Klein Tank et al. 2009). It has been noted that other synonyms, similar in meaning to "extreme," may be used interchangeably, such as "severe," and "exceptional." Generally, the traditional drought index possesses percentile-based extreme-value categorization that is applied to a one-dimensional time series. Taking the standardized precipitation index (SPI)/standardized precipitation evaporation index (SPEI) for example, the severe and extreme drought are initially defined as the time-scale-specific sequences less than –1.5 and –2, respectively corresponding to the 6.7th and 2.3rd percentiles. By doing so, most previous studies naturally imported the way to extract extreme events. Hence, this key issue receives little attention and has not been critically examined, as the task seems particularly simple and effortless. Unfortunately, the definition of extreme drought is much more complex than it first appears, because a critical issue in the study of drought, unlike heatwaves or heavy precipitation, is its multiscalar nature. Specifically, the multiscalar nature of drought refers to that the response of usable water resources, including soil moisture, groundwater, snowpack, river discharges, and reservoir storages to water shortage varies markedly and with different time scales (Beguería et al. 2010;

Hayes et al. 2011). It implies that the categorization of extreme drought would only make sense in reference to a particular time scale. As such, it is common to find extreme drought conditions recorded in one system (e.g., low river flows), whereas other systems in the same region (e.g., crops) have normal or even humid conditions (Vicente-Serrano et al. 2011, 2012). This makes it hard to define extreme drought event, since different water resources component can be heterogeneous within a region. To account multiscalar nature, Wang et al. (2016) prompted integrated treatment of drought and sparked the early form of super drought concept, whose task is to judge whether SPEI at multiple time scales are all below −1.5. However, such a concept and related indicator are indeed qualitative and far less effective in assessing the magnitude and patterns, and only have been achieved at specific regional scale. Motivated by this gap, the objective of the present research is establishing the theoretical basis of super drought and developing a quantitative index, as well as replicating the success on a global scale. In the next paragraph, we review a variety of quantitative ways devoted to combining multiple drought indices (Hao and Singh 2015) although not targeted toward super drought detection.

Linear combination is a natural choice to combine different drought variables or indices to integrate drought information, e.g., Mo and Lettenmaier (2014), Hao et al. (2016), Xia et al. (2014), Zhang et al. (2017), Keyantash and Dracup (2004), Rajsekhar et al. (2015), and Waseem et al. (2015). Although linear combination is generally easy to implement, it fails to characterize the covariability of drought-related variables, which may interact in a complex manner (Hao and Singh 2015). Copula is an effective way to solve the complicated and nonlinear relationship among multiple variables (Hofert et al. 2018). The first attempt of application of copula in constructing probability-based overall water deficit index was made by Kao and Govindaraju (2010). They developed the joint deficit index via empirical copula to join accumulated precipitation or streamflow with temporal scales varying from 1 to 12 months, in order to capture both short- and medium-term droughts. The similar copula framework is utilized by Hao and AghaKouchak (2013), Ma et al. (2014, 2015), Yang et al. (2018), Shah and Mishra (2020), and others.

Based on the above review, the copula technique is increasingly popular in modeling a joint drought index. While copula-based joint index modeling made substantial progress in the past decade, creating a comprehensive copula-based framework dealing with super drought detection is still far from complete. First, copula is a general tool, so it is paramount to identify how best to tailor it to super drought quantification. Second, in order to be well suited for the high-dimensional feature space of drought, we implement the advanced vine copula theory instead of classic copula to evade the curse of dimensionality. Third, the properties and true validation of the established joint index have not been well documented. This study will give a comprehensive perspective to achieve the goals for understanding the superiority of the novel index and the super drought concept. Last, unlike most of previous works conducted at regional scales, this study provides global-scale modeling and verification so as to guarantee a universally applicable concept and index.

In this study, we build a theoretical basis for super drought and propose a novel framework based on vine copula and the associated monitoring index. This paper is structured as follows. The second section introduces the data sources. The third section describes the background and motivation to develop the concept of super drought. The fourth section is the core part of this study, which details the procedure and specific settings to build the monitoring index called the comprehensive multiscalar index (CMI). The properties of CMI and associated super drought are interpreted in the fifth section. The sixth section is conducted to validate the performance of CMI and super drought recognition. Finally, the discussion and conclusions are made in the seventh and eighth sections, respectively.

Data

CRU precipitation and potential evapotranspiration. Monthly precipitation and potential evaporation (PET; units: mm) are obtained from the latest version TS4.05 of Climatic Research Unit (CRU; Harris et al. 2020). PET data are estimated by the Penman–Monteith parameterization scheme (Allen et al. 1994). CRU TS4.05 data are month-by-month variations over the period 1901–2020, provided on a 0.5° × 0.5° horizontal grid extending over the global land. In the "Validation of CMI" section, the worldwide skill of CMI will be testified against GRACE data, which is the only option to use at a global scale. Therefore, to match the true resolution of GRACE, the high-resolution CRU data are transformed to 3° resolution through conservative regridding. It should be mentioned that upscaling to the coarse pixel scale is undertaken for validation purposes, but not intended for drought characteristics evaluation. Once the novel algorithm and index are established and justified, the original 0.5° data source is placed back to produce a high-resolution map and restore fine-scale features.

Given the relatively poor quality and low spatial density of in situ measurements in the earlier part of the twentieth century, a period of 60 years from 1961 onward is used. In addition, extra treatment is performed in regard to this drought study, as explained below. To account for the intrinsic multiscalar nature of drought, raw values are accumulated to multiple time scales up to 48 months. However, this aggregation procedure will result in data gaps at the beginning of the accumulated time series. For example, at the longest 48-month time scale, the first 47 months of the accumulated time series are not defined. To avoid the missing data problem, the CRU data are extended back from the start date January 1961 to the previous 47 months. After implementing accumulation, the months before January 1961 are discarded, so that the study period 1961–2020 is not altered with the advantage of no null values contained.

In addition, the global land-cover map V2.3 compiled by the European Space Agency are used to exclude desert areas.

SPEI. Prior to describe the concept of super drought and the newly developed index CMI, it is necessary to outline the broadly used SPEI (Vicente-Serrano et al. 2010). SPEI can be calculated on a range of time scales, over which water deficits accumulate is vital to separate different types of droughts. In this study, the SPEI were calculated with various lags including 3, 6, 12, 24, and 48 months recommended by McKee et al. (1993). SPEI values can be classified into four drought classes, namely, mild or near normal (0 to −0.99), moderate (−1.00 to −1.49), severe (−1.5 to −1.99), and extreme (−2 and below). The theoretical probabilities of SPEI less than −1.5 and −2 are 6.7% and 2.3%, respectively.

GRACE total terrestrial water storage. The total terrestrial water storage (TWS), expressed in terms of equivalent water thickness (unit: cm), is obtained from Gravity Recovery and Climate Experiment (GRACE) satellite observations (Tapley et al. 2019). GRACE detects the spatiotemporal variation of the global gravity field. After removing atmospheric masses, GRACE gravity changes correspond mainly to the variations in TWS, which is the sum of all above and below surface water storages, including canopy water, rivers and lakes, soil moisture, and groundwater.

In this study, we retrieve the latest GRACE mascon product release 06 (RL06) compiled by the Center for Space Research (Save et al. 2016). The product has undergone all the appropriate corrections, including C20 (degree-2, order 0) and C30 (degree-3, order 0) replacements, degree-1 correction and GIA (glacial isostatic adjustment) correction. For further details on the calibration strategy, see section S1 of the online supporting information (https://doi.org/10.1175/BAMS-D-22-0182.2). For the temporal dimension, the dataset spans from January 2002 to the present at monthly intervals. For the spatial dimension, the dataset is provided

with a spatial sampling of 0.5°. However, the native resolution of the GRACE mascon solution is actually 330 km, or equivalently a 3° spherical cap (Landerer and Cooley 2021). As such, the initial 0.5° × 0.5° spatial resolution is upscaled to 3° × 3° with the area conservative remapping method.

Motivation and concept of super drought

Problem overview and motivation. In the introduction section, we have explained in theoretical consideration why it is challenging to arrive at a definition of extreme drought. This section carries out real-world evaluation to assess the degree to which the multiscalar nature obscures the extreme drought definition.

We use the time series at the grid point (49.5°N, 13.5°E) to illustrate the common problem of defining extreme drought, as shown in Fig. 1. The grid point is arbitrarily selected as an example to highlight the discordance of drought conditions among different time scales. In fact, such a trait appears to be a common consequence of multiscalar drought, irrespective of geographic location and local climate characteristics, as evidenced by the global examination in Fig. 2. More cases to display the effect of time scales are shown in section S2 of the supporting information, including not only drought index but also direct measurements of drought on different water resource components.

It has become clear and visible how the dry and wet states act differently, and sometimes opposite, across different time scale. Further, we select three representative time nodes representing November 1982, August 2018, and October 2020, as marked in Fig. 1. The corresponding SPEI values at the five time scales are [–2, –1.4, –1.3, 0.073, 1.2], [–1.8, –2.1, –1.7, –1.6, –1.9], and [1.2, 0.62, –0.34, –1.3, –2.1] for the three cases.

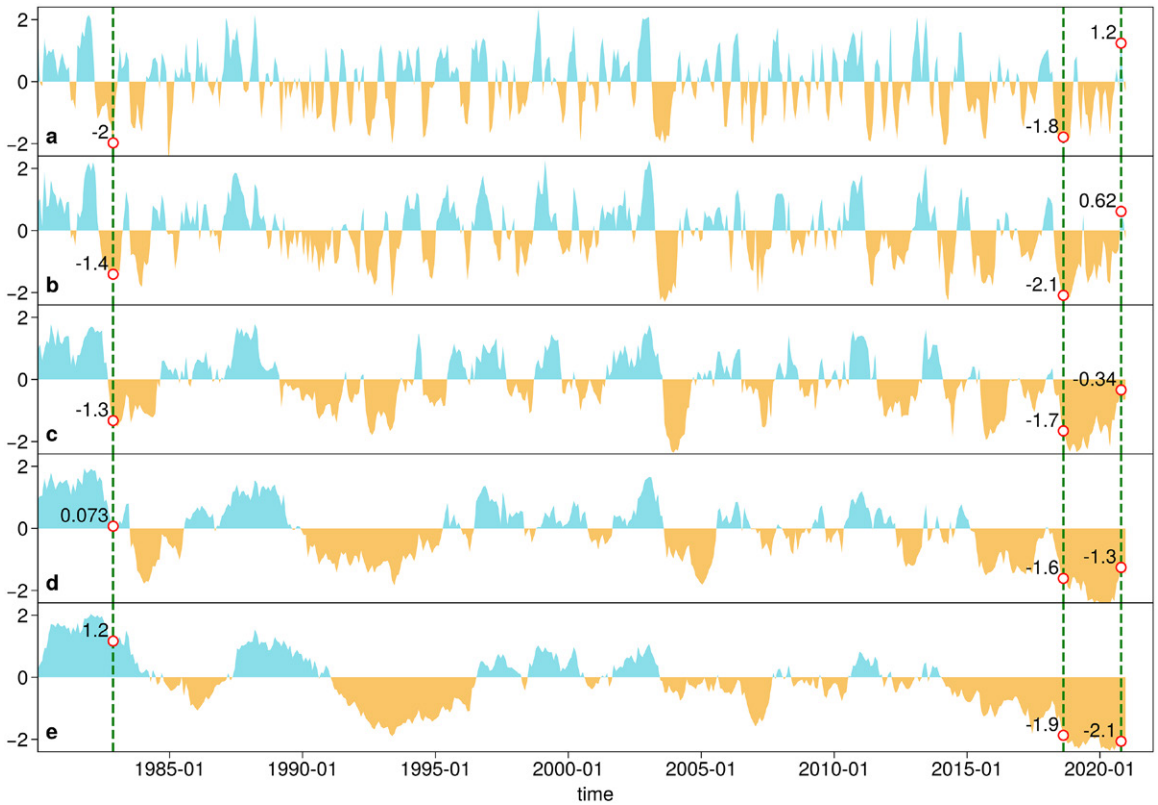

Fig. 1. Example of temporal evolution of SPEI at the grid point (49.5°N, 13.5°E) for time scales of (a) 3, (b) 6, (c) 12, (d) 24, and (e) 48 months from January 1980 to December 2020. The values in November 1982, August 2018, and October 2020 are marked with dashed lines. Note that the SPEI time series are calculated over the period of 1961–2020, but only the period since 1980 is reported here as an example.

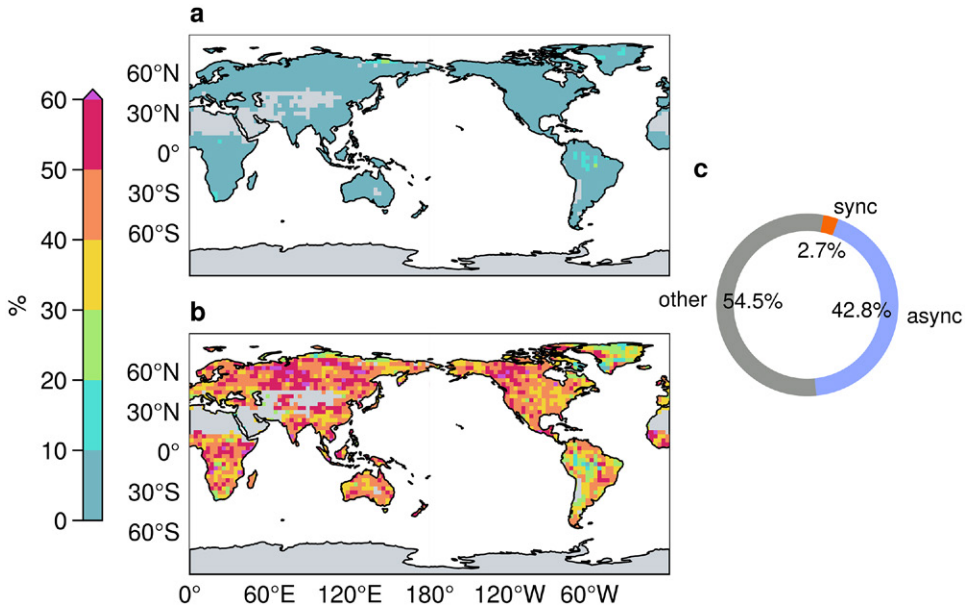

Fig. 2. Spatial patterns of the percent of (a) synchronous and (b) asynchronous occurrences of severe drought at multiple time scales, and (c) the corresponding donut chart summarizing the spatial data. Refer to the main text for the definition of synchronous and asynchronous as well as other groups.

For November 1982, the SPEI at 3-month time scale falls in the extreme drought category. However, it can only be concluded that the 3-month SPEI is affected by extreme drought, because the 24- and 48-month SPEI values are 0.073 and 1.2, respectively, indicative of a humid condition. October 2020 revealed a similar but reversed pattern of SPEI. Both cases illustrate that the dry and wet periods for different drought of hydrological components are not synchronous, and sometimes even opposite. On rare occasions, there exists the simultaneous occurrence of extreme droughts at multiple time scales. For example, August 2018 is the episode of concurrent severe dryness, as indicated by all SPEI values below −1.5.

We then calculate the percentage of synchronous and asynchronous occurrences over the globe. Denote by $\mathbf{W} = \{\mathbf{p}(p_1, p_2, p_3, p_4, p_5) | \exists p_j < -1.5\}$, the whole set that has at least one time-scale SPEI in the severe category, $\mathbf{S} = \{\mathbf{p}(p_1, p_2, p_3, p_4, p_5) | \mathbf{p} \in \mathbf{W}, \forall p_j < -1.5\}$, the subset of $\mathbf{W}$ that has all time-scale SPEI under the severe category, $\mathbf{A} = \{\mathbf{p}(p_1, p_2, p_3, p_4, p_5) | \mathbf{p} \in \mathbf{W}, \exists p_j > 0\}$, the subset of $\mathbf{W}$ that has at least one time-scale SPEI under humid conditions. The rest, not belonging to any of the above categories, will be allocated to the subset called "other," $\mathbf{O} = \mathbf{W} \backslash (\mathbf{A} \cup \mathbf{S})$, but it is clearly not our concern. Then, the percentages of occurrence assigned to subset $\mathbf{S}$ (synchronous) and $\mathbf{A}$ (asynchronous) are calculated in each grid cell and then summarized globally, as shown in Fig. 2.

Figure 2a shows that the percentage of synchronous droughts is less than 10%. The definite fraction of such events among the total events is estimated, globally averaged, to be 2.7% (Fig. 2c). To better reflect the spatial differentiation, Fig. 2a is duplicated but with a different color scheme, as shown in Fig. S2 in the supporting information. The result indicates that a very low rate of multiscalar severely drought turned out to coincide. However, the opposite phenomena, asynchronous events, as shown in Fig. 2b, exhibit much higher frequency, with uneven regional distribution ranging from 30% to 60%. On average, asynchronous events occur 42.8% of the time (Fig. 2c), which is far more often than the synchronous counterpart.

This testing goes further to examine the conditional probability that severe drought at one time scale will occur, given the presence of another time scale's event. As an example, we

take the 3- and 24-month time scales to represent meteorological and hydrological processes. With real-world assessment, the probability of severe meteorological drought is found to be 22% when hydrological drought has already occurred. Yet, in spite of increased likelihood relative to the theoretical one (6.7%), there is an equal chance (22%) that meteorological wet conditions occur. In this regard, a hydrological severely dry state cannot guarantee meteorological severely dry state, and vice versa. Therefore, conditional probability is also not adequate to express the likelihood with which multiple events co-occur.

In sum, the extreme drought and wet condition are much likely to coexist, rendering the distinction between extreme and nonextreme event difficult. As such, it is critical to establish a concept and criterion in what can be ranked as an extreme drought event.

Concept of super drought. We have known the fact that the phases and frequencies of dry–wet oscillations at different time scales all differ; at times they are opposite and at other times they coincide. It is conceivable that a devastating event appears when extreme phases of short- and long-term droughts coincide. Therefore, the concept of super drought referred to the simultaneous occurrence of extreme droughts at multiple time scales. In a physical sense, super drought can be regarded as compound water deficits in all parts of usable water resources, which is expected to reinforce the damage that would result from a single-time-scale event. The situation is clearly the case in August 2018 (Fig. 1). Conversely, if the extreme droughts at different time scales occur in isolation, the destructive effect of the droughts may not be as serious. For instance, the drought impact during October 2020 and November 1982 tended to be gentle, despite severe drought status at part of the time scales.

A schematic diagram Fig. 3 was constructed to better illustrate the super drought concept. The drought condition for the month of interest (labeled as n) depends not only on the event on the current month but also the preceding months ($n - 1$, $n - 2$, ...) up to a certain time scale. Time scale refers to the number of months extending through the end of the current month. Since droughts of different time scales have diverse impacts including meteorological,

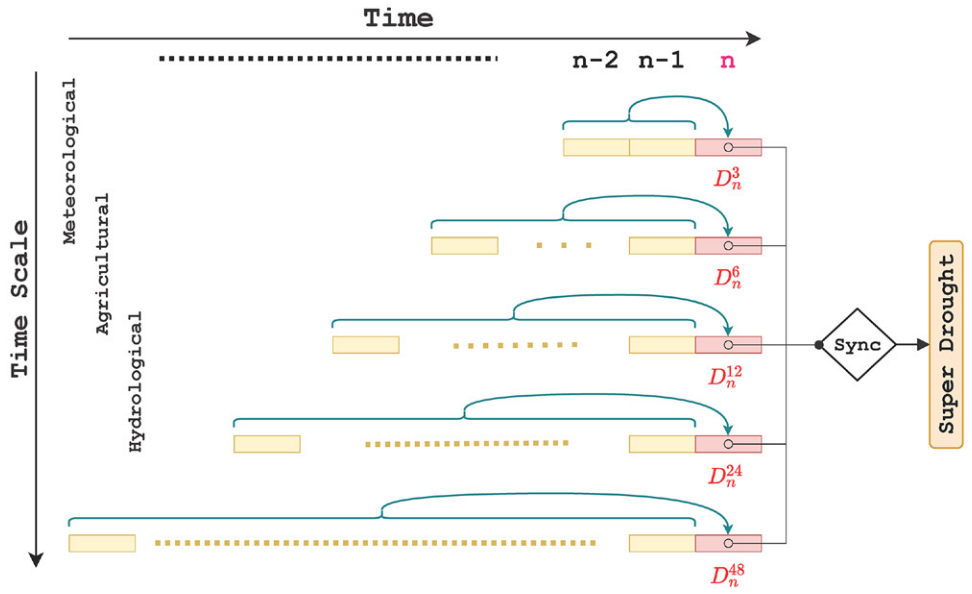

Fig. 3. Schematic diagram of the super drought concept. The rightward arrow on the top denotes the evolving time, while the time scale from short term to long term is represented by the downward arrow on the left. The month of interest is colored in a red block and the preceding months up to a certain time scale are colored in yellow blocks and dots. The number of dots signals the number of month blocks omitted. Six illustrative time scales involve 3, 6, 12, 24, and 48 months, with D_n^3, D_n^6, D_n^{12}, D_n^{24}, and D_n^{48} denoting the cumulative water balance at the corresponding time scale.

agricultural, and hydrological forms, the cumulative water deficit or surplus can be calculated across various months. The notation D_n^k is employed to denote the accumulated value starting from the current month n and adding the preceding $k-1$ months, where k corresponds to the desired time scale of the aggregation. For instance, the 6-month D_n^6 is constructed by the sum of the water status from 5 previous months to the current month. In this study, 3-, 6-, 12-, 24-, and 48-month windows are used to reflect short-term, medium-term, and long-term conditions. Here, it is important to note that the time scale does not measure drought length; rather, it serves as an aggregation scheme to quantify dry/wet state at one point in time. Specifically, D_n^k captures the influence of the climatic water balance conditions of the preceding $k-1$ months on the current month (n). As shown in Fig. 3, for the specific month n, it is possible to experience dry condition on one or more time scales and wet conditions at other time scales. This clearly poses a difficult situation to convey extreme drought events. Consequently, the super drought concept is designed to express the synchronous occurrence of extreme drought across multiple time scales.

At the same time, it is necessary to explain why we have chosen to use the terminology "super drought." In most previous studies, the terms "extreme drought," "exceptional drought," "massive drought," and "megadrought" are usually used. In comparison, the term "super drought" has no specific definition in scholarly literature, despite being used frequently in social media as a general description. In this study, we definitely coin the term "super drought" as simultaneous occurrence of extreme droughts at multiple time scales. The term "super drought" could be the ideal choice in the context. On the one hand, the word "super" means "beyond," "greater," or "on top of" (as in "superior"), referring to a higher level of destruction than each individual component. On the other hand, the word "super" also provides a sense of "superimposed," referring to the synthetic effect of each individual component.

As a summary, the physical significance of the super drought concept represents the combination of multiple stresses on water resources, or in other words the grand deficit in total usable water resources.

CMI and super drought detection based on vine copula

With the concept of super drought, how does one work out a quantitative index for determining the overall extremity? In this section, we employ vine copula theory to develop a novel index called CMI in ways that are tailored to super drought detection. Meanwhile, it is necessary to spare a little space to explain the background for adopting "comprehensive multiscalar index" as the novel index name. Our previous study (Wang et al. 2016) sparked the early form of super drought concept and proposed a qualitative indicator called comprehensive multiscalar indicator. In that work, the term "indicator" expresses a qualitative judgment, which is claimed to be either true or false. One objective of the current study is to develop a quantitative index for super drought characterization, which greatly improves and extends the previous approach. In this sense, "comprehensive multiscalar index" becomes the natural choice and thus can be regarded as the quantitative version of "comprehensive multiscalar indicator," which helps to maintain coherence and standardization of terms that are being used across a series of studies.

Copula and vine copula theory to measure the overall water deficit from multiscalar drought. First, we introduce the copula and vine copula theory, with emphasis on integrating multiscalar aspects of drought. The copula model was first introduced by Sklar (1959), and a more recent copula theory can be found in Nelsen (2007). In short, a copula is a multivariate cumulative distribution function where the marginal probability distribution of each variable is uniform. Assuming dry–wet status at two distinct time scales as random

variables X and Y, respectively, the two-dimensional joint cumulative distribution can be expressed as

$$\mathbb{P}\left(X \le x, Y \le y\right) = C\left[F\left(x\right), G\left(y\right)\right], \tag{1}$$

where C is the copula, and $F(x)$ and $G(y)$ are the marginal cumulative distributions that are uniform. The comma inside the parentheses stands for two conditions being simultaneously true. The principle can be readily extended to more than two variables, that is,

$$\mathbb{P}\left(X_1, X_2, ..., X_d\right) = C\left[F_1\left(X_1\right), F_2\left(X_2\right), ..., F_d\left(X_d\right)\right].$$

An example given in Eq. (1) based on the normal copula with linear correlation of 0.5 is displayed in Fig. 4. In this graph, the marginals describe the respective characteristics, while the copula contours evaluate the joint behavior. We define the percentile range from 0 to 1 spanning the range from wet to dry conditions. The three points representing the three combinations of X and Y with different marginal percentiles are marked in Fig. 4, namely, P1(0.9, 0.3), P2(0.3, 0.9), and P3(0.9, 0.9). Considering dry extreme is defined as the upper 90th percentile of the distribution. P1 corresponds to the condition in which X shows extreme drought, while Y does not, and P2 refers to the opposite case. However, they possess the same composite effect with the copula value being 0.29, suggesting overall normal to wet conditions. In contrast, P3 features that both X and Y are under extreme drought, resulting in compound dry stresses with joint risk abruptly soaring to 0.83. It indicates that if both X and Y exceed a threshold (P3), it will lead to a more severe drought than one agent working alone (P1 or P2). In addition, section S4.1 of the supporting information is presented to explain why nonexceedance copula $\mathbb{P}\left(X \le x, Y \le y\right)$ should be used instead of exceedance copula $\mathbb{P}\left(X > x, Y > y\right)$.

In conclusion, copula is capable of computing a probability-based overall water deficit. In addition, it is worth noting here that the Kendall rather the copula value is eventually used to measure the joint probability, but it does not change the basic principle. To keep the integrity of this study, the definition and significance of Kendall measure will be presented in the "Specific settings tailored to super drought monitoring" section.

With the above knowledge, it seems natural to extend the bivariate copula to high dimension for overall multiscalar drought characterization, which is a multidimensional rather than two-dimensional problem. But unfortunately, the direct extension of copula to high orders suffers from the "curse of dimensionality" (Kao and Govindaraju 2008). Even worse, although the catalogue of bivariate parametric copula families is large, this is not the case for dimensions larger than 2. To address the issues, vine copula, introduced by Joe (1996), is developed to

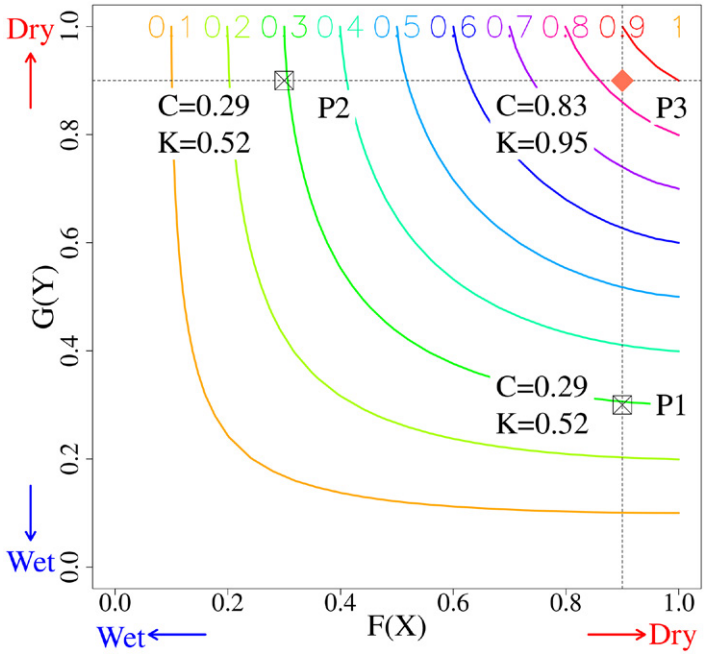

Fig. 4. The bivariate normal copula with linear correlation $\rho = 0.5$. The overlaid points at P1(0.9, 0.3), P2(0.3, 0.9), and P3(0.9, 0.9) show the copula value (*C*) and Kendall measure value (*K*).

decompose high-dimensional copula into a cascade of bivariate copulas. The mathematical form of the decomposition can be written as (Aas et al. 2009)

$$\begin{aligned} f\left(x_1,\ldots,x_d\right) &= f\left(x_d\right)\cdot f\left(x_{d-1}\middle|x_d\right)\cdot f\left(x_{d-2}\middle|x_{d-1},x_d\right)\ldots\cdot f\left(x_1\middle|x_2,\ldots x_d\right) \\ f\left(x\middle|\boldsymbol{\upsilon}\right) &= c_{x\upsilon_j|\boldsymbol{\upsilon}_{-j}}\left\{F\left(x\middle|\boldsymbol{\upsilon}_{-j}\right),F\left(\upsilon_j\middle|\boldsymbol{\upsilon}_{-j}\right)\right\}\cdot f\left(x\middle|\boldsymbol{\upsilon}_{-j}\right), \end{aligned} \tag{2}$$

where $c_{x\upsilon_j|\boldsymbol{\upsilon}_{-j}}$ is the copula density, υ_j is an arbitrary component of $\boldsymbol{\upsilon}$, and $\boldsymbol{\upsilon}_{-j}$ denotes the vector $\boldsymbol{\upsilon}$ excluding υ_j. Obviously, the same multivariate density can be expressed by a large number of different vine copulas with different tree structures and orderings of variables. The detailed theory is available in Kurowicka and Joe (2011) and Czado (2019). Thereby, vine copula provides an adaptable and manageable way to construct the joint distribution of multiscalar droughts. All candidate bivariate copula families to build vine are listed in Table 1.

Procedure to construct the novel CMI based on vine copula. In this part, we create a novel and systematic framework based on vine copula to probabilistically integrate multicomponent metrics of drought into an integrated metric CMI. There are three main stages to construct CMI and detect super drought.

Step 1: Data preparation and preprocess
Step 2: Vine copula construction and goodness-of-fit test
Step 3: CMI derivation and super drought detection

A sequential flowchart is elaborated in Fig. 5. Note that this process is carried out for each calendar month of each grid cell. The vine copula construction is implemented in the exemplary grid cell (49.5°N, 13.5°E) as a case study to give a clear perception of the methodology, which is documented in section S3 of the supporting information.

Step 1: Data preparation and preprocess. Based on precipitation and PET, water balance accumulated at various time scales is formulated as

$$D_n^k = \sum_{i=0}^{k-1}\left(\mathrm{PET}_{n-i} - P_{n-i}\right), \quad n \geq k, \tag{3}$$

Table 1. Candidate bivariate copula families.

Type	Name (abbreviation)	Rotations (°)	No. of parameters
—	Independence (I)	—	0
Elliptical	Normal/Gaussian (N)	—	1
	Student *t* (t)	—	2
Archimedean	Clayton (C)	90, 180,[a] 270	1
	Gumbel (G)	90, 180, 270	1
	Frank (F)	—	1
	Joe (J)	90, 180, 270	1
	Clayton–Gumbel (BB1)	90, 180, 270	2
	Joe–Gumbel (BB6)	90, 180, 270	2
	Joe–Clayton (BB7)	90, 180, 270	2
	Joe–Frank (BB8)	90, 180, 270	2

[a]A copula rotated by 180° is often called a survival copula.

where k is the time scale and n is the month. Note that the water balance defined here is the opposite of the traditional definition, which will be explained in the "Specific settings tailored to super drought monitoring" section. In this study, five time scales (k = 3, 6, 12, 24, 48) recommended by McKee et al. (1993) are used. The reason will be explained in the "Specific settings tailored to super drought monitoring" section.

Combing with the fact that copula is defined as distribution function whose marginal distributions are uniform in the interval [0, 1], the conversion of marginal uniformity is achieved by using the empirical probability integral transform (PIT):

$$\begin{aligned} &\mathbf{x}_j = \left(x_{1j}, x_{2j}, \ldots, x_{nj}\right)^{\mathrm{T}} \rightarrow \mathbf{u}_j = \left(u_{1j}, u_{2j}, \ldots, u_{nj}\right)^{\mathrm{T}}, \quad j \in \{1, \ldots, d\} \\ &u_{ij} = r_{ij} \Big/ \left(n+1\right), \quad i \in \{1, \ldots, n\}, \forall_j \end{aligned} \tag{4}$$

where r_{ij} denotes the rank of x_{ij} among all x_{kj}, $k \in \{1, \ldots, n\}$. In the copula literature, values obtained by the PIT are called pseudo-observations.

Step 2: Vine copula construction and goodness-of-fit test. At the core of the methodology lies modeling of vine copula, which consist of a tree-based hierarchy of conditional bivariate copulas. This study implements the flexible tree structure known as regular vine (R-Vine), which is a powerful graphical tool to characterize complex dependence among multiple variables (Bedford and Cooke 2002). Formally, fitting an R-Vine copula specification to pseudo-observations requires the following three tasks: (i) selection of the R-Vine structure, that is, choosing and connecting the most dependent pairs in the tree; (ii) choice of a bivariate copula family for each pair and estimation of the corresponding parameters; and (iii) a goodness-of-fit test.

We first proceed to select the appropriate R-Vine structure, which requires correlation between studied signatures. Rank correlation coefficients defined by the empirical Kendall's τ between all pairwise variables are

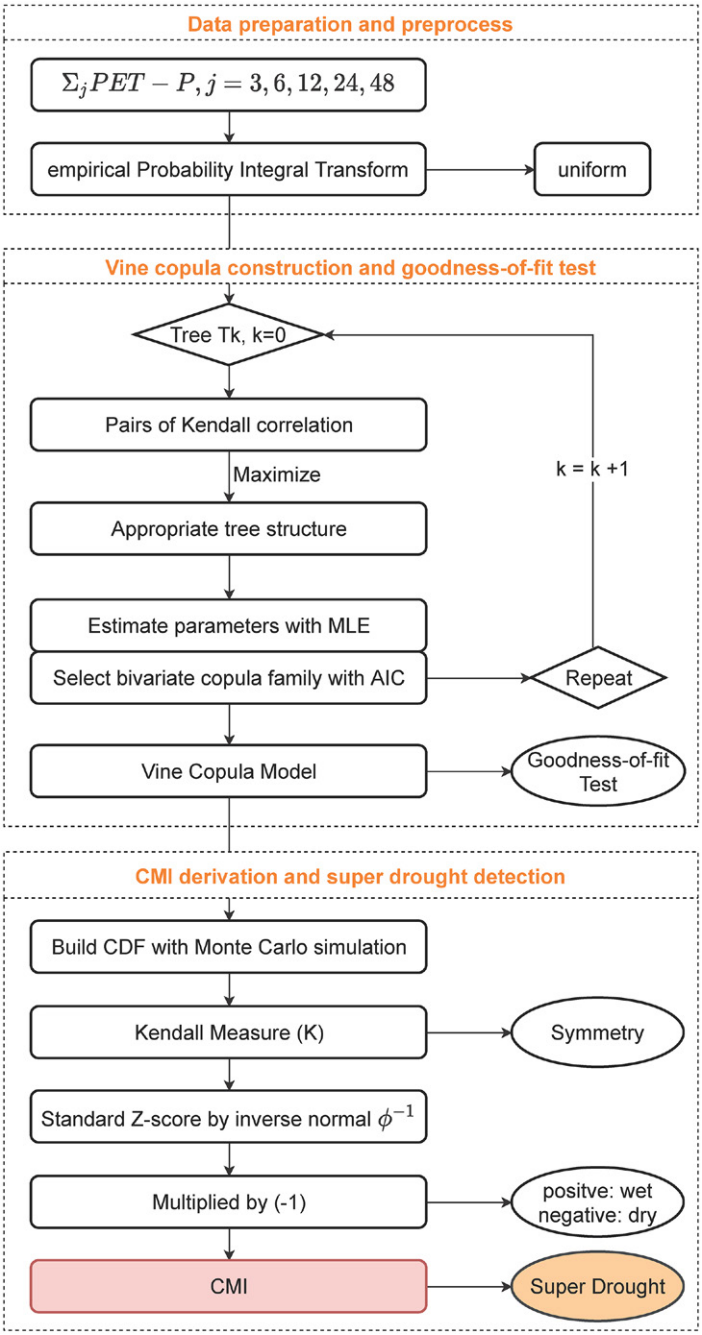

Fig. 5. Flowchart of CMI construction and super drought detection based on vine copula.

computed, so as to recognize the spanning tree that maximizes the sum of absolute empirical Kendall's τ. The Kendall's τ coefficient of X and Y is written as

$$\tau_{XY} \in [-1,1] = \mathbb{P}\left[\left(X_1 - X_2\right)\left(Y_1 - Y_2\right) > 0\right] - \mathbb{P}\left[\left(X_1 - X_2\right)\left(Y_1 - Y_2\right) < 0\right], \tag{5}$$

where (X_1, Y_1) and (X_2, Y_2) are two independent and identically distributed copies of (X, Y).

Having selected the appropriate order of the variables, in what follows, identifying the bivariate copula type and the corresponding parameters that best fit the observations is the most crucial part. To this end, all candidate copula models listed in Table 1 are fitted to the same data with parameters determined based on maximum likelihood estimation (MLE), and then the Akaike information criterion (AIC) is computed for each model. In symbols, the parameter estimation and AIC (Akaike 1998) are defined as

$$\begin{aligned} \hat{\boldsymbol{\theta}} &= \arg\max_{\boldsymbol{\theta}} \sum_{i=1}^{n} \ln\left[c\left(u_{i1}, u_{i2} \middle| \boldsymbol{\theta}\right)\right] \\ \mathrm{AIC} &= -2\sum_{i=1}^{n} \ln\left[c\left(u_{i1}, u_{i2}\right) \middle| \hat{\boldsymbol{\theta}}\right] + 2k, \end{aligned} \tag{6}$$

where $\{(u_{i1}, u_{i2}), i = 1, \ldots, n\}$ are pseudo-observations, c is the copula density, and k is the number of parameters in the model. The lower the AIC values, the better the model. As such, we select the best-fit copula family, which has the lowest AIC value.

The ultimate result of the case study is shown in Fig. 6, portraying the tree sequence together with copula family and parameters. Under the above procedure, vine copula is trained to observations independently for each grid cell and each calendar month.

After fitting the vine copula to samples, it is imperative to test the effectiveness of the proposed model. The goodness-of-fit (GOF) test is intended to test the validity of the null hypothesis $H_0 : C \in \mathcal{C}_0 = \{C_{\boldsymbol{\theta}} : \boldsymbol{\theta} \in \Theta\}$ against $H_1 : C \notin \mathcal{C}_0$, where C denotes the vine copula distribution function and $\mathcal{C}_0$ is class of parametric vine copula with Θ being the parameter space. There are different GOF tests proposed, as reviewed in Schepsmeier (2015). Here we use Rosenblatt's transform test, which projects the multivariate problem to a univariate problem and then applies a univariate test. The algorithm is provided in the section S4.2 of the supporting information.

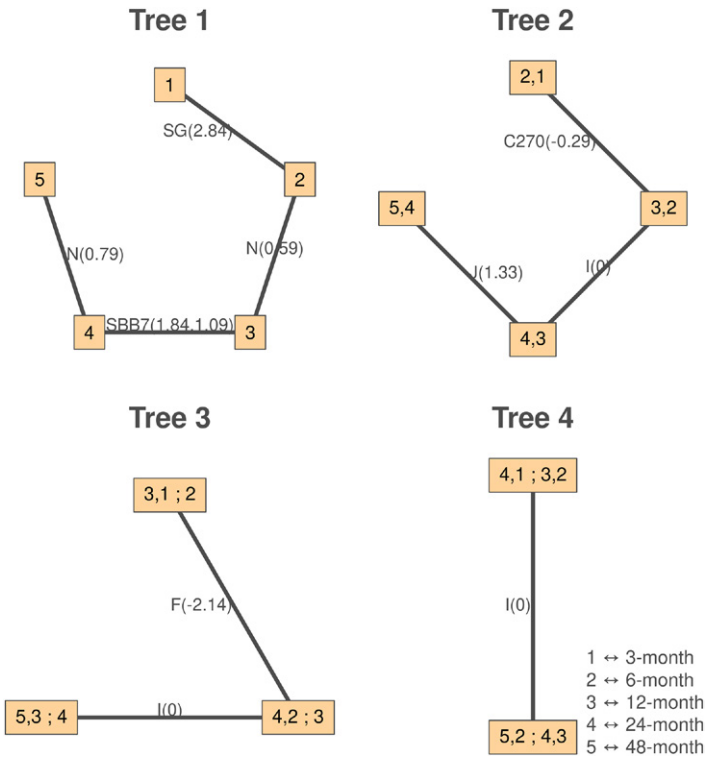

Fig. 6. Tree sequence for the estimated vine structure for the case study. Each edge in the vine graph is associate with the best-fit copula family and fitted parameters in brackets, where SG is survival Gumbel, N is normal, SBB7 is survival Joe–Clayton, C270 is rotated Clayton (270°), J is Joe, F is Frank, and I is independence. Labels 1, 2, 3, 4, and 5 represent the 3-, 6-, 12-, 24-, and 48-month time scales, respectively.

The result of GOF test is shown in Fig. 7, which depict the p value of the test. Choosing a threshold of 0.1, a large p value and hence failure to reject the null hypothesis is a good result. The spatial

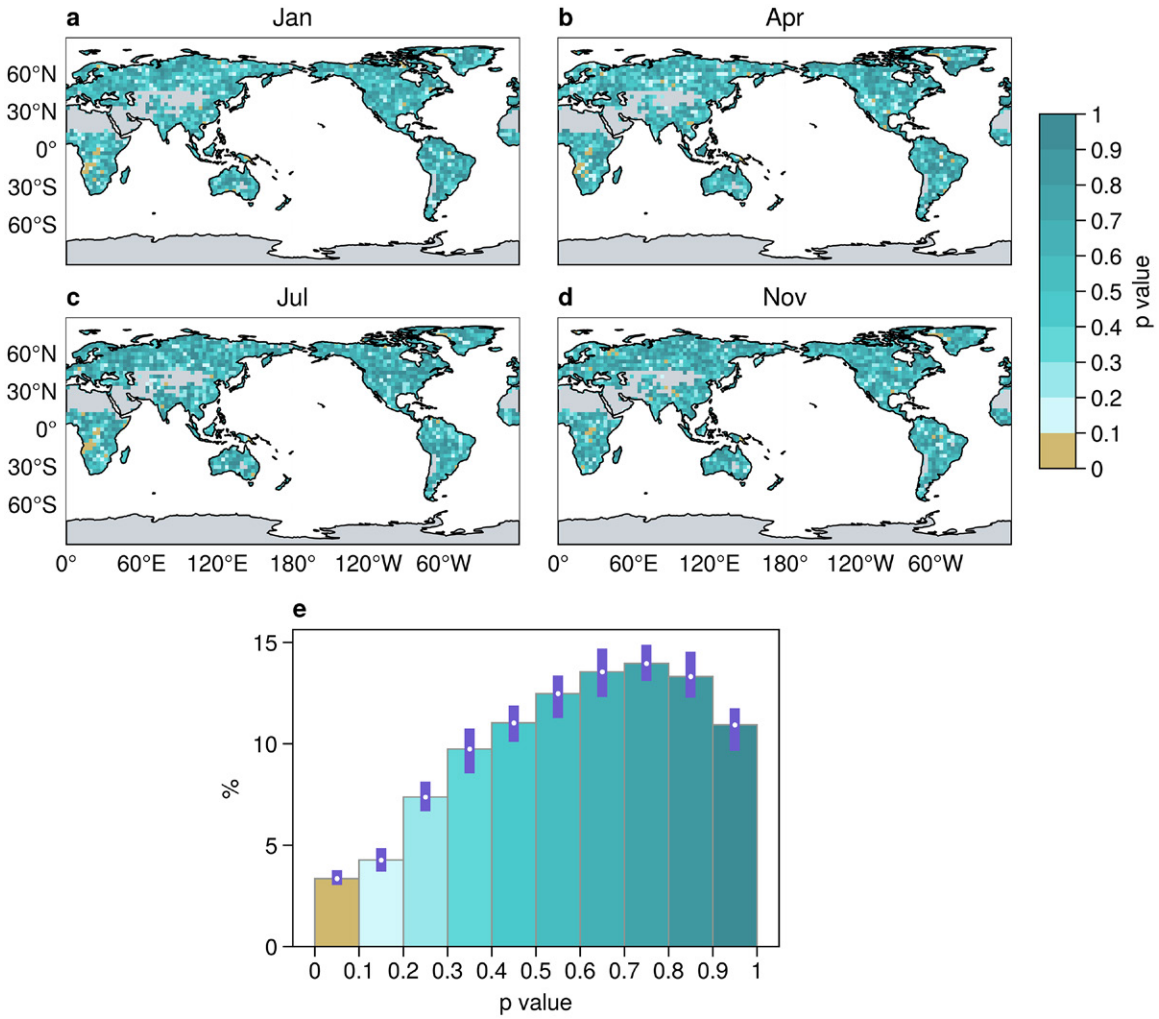

Fig. 7. The *p* values for the goodness-of-fit test for vine copula based on the Rosenblatt's transform, described in (a)–(d) the spatial patterns for January, April, July, and November, respectively, and (e) a histogram over all grid points and calendar months. The error bars in (e) represent the 5%–95% confidence interval across all calendar months.

patterns (Figs. 7a–d) demonstrate considerable confidence in the potential of vine copula for robust fitting over almost all corners of the global land, irrespective of climatic zone and the calendar month. Only for very few areas does the fitted vine copula model fail to match the observations. Further, a histogram is drawn to show the frequency distribution of p values. As seen from Fig. 7e, the p values are well above 0.4, as the percentage oscillates between 73% and 78%. The rejection rates of null hypothesis only account for less than 4%. In addition, the short error bar length shows little dependence of the performance on the seasonality. In conclusion, the vine copula is highly appropriate for modeling the joint distribution of multiscalar drought.

Step 3: CMI derivation and super drought detection. Although the vine copula model is built, it is copula density function (c) rather than copula distribution function (C) that has been established. However, there is no easy way to derive the analytic expression of C, which involves a $(d-2)$-dimensional integral. To get rid of the difficulty, a Monte Carlo simulation is carried out to numerically construct C given by its density c. In application, 50,000 Monte Carlo samples are used to guarantee the estimator of the target C is precise enough.

With the distribution function C, it seems likely that the final standardized score can be readily obtained by taking the inverse normal distribution function, as used in SPEI. Unlike univariate cases, however, it is necessary to make a transformation from copula

measure to Kendall measure via Kendall function (Nelsen et al. 2003). The reason will be further detailed in the "Specific settings tailored to super drought monitoring" section. Kendall function is designed to describe the distribution functions of copula values in the whole measure space:

$$K(q) = \mathbb{P}\left[C_{U_1,\ldots,U_d}(U_1,\ldots,U_d) \le q\right], \quad q \in (0,1). \tag{7}$$

In the final step, the standardized score can be computed based on the Kendall measure by taking the inverse normal Φ^{-1}. In addition, reminding the input logic to calculate CMI is PET minus precipitation, so we reverse the sign of the standardized score to conform to the traditional paradigm in the drought index community. The final CMI is defined as

$$\mathrm{CMI} = (-1)\cdot\Phi^{-1}(K). \tag{8}$$

Such a standardization algorithm makes the CMI follow a standardized normal distribution. Compared to SPEI, the proposed CMI incorporates the overall drought conditions reflected from multiscalar components. The negative CMI indicates joint dry status, while positive CMI represents an overall wet condition. A CMI near zero refers to overall normal condition. Based on CMI, we can set −1.5, −2, or other values as the threshold for identifying super drought events.

Specific settings tailored to super drought monitoring. Although the vine copula model provides a universal structure to model the multidimensional distribution, we need to tailor it to the specific requirements of super drought configuration and CMI establishment with a focus on concordant extreme events. The four key settings for the goal include (i) input logic of water balance definition, (ii) optimal selection of time scales, (iii) vine layout, and (iv) Kendall measure. Here, we only report the major conclusion, while further details are provided in section S4.3 of the supporting information.

As regards the input logic [setting (i)], the choice between PET–P or P–PET does matter in copula-based modeling which involves nonlinearity. Although P–PET is always the traditional choice in defining water balance, it is identified that PET–P could better highlight overlapping drought, known as super drought, compared to nonoverlapping type. Therefore, we reverse the traditional order of the water balance definition to yield PET–P as the input logic to the copula model. Selection of appropriate time scales that the copula model joins [setting (ii)] is one of the important topics to consider. We confirm that including the time scales of 3, 6, 12, 24, and 48 months is adequate for allowing an accurate detection in a very reduced computation time. In our question of multiscalar drought, the D-vine structure characterized by one path that goes through all the nodes [setting (iii)] is especially appropriate to be selected for the temporal-scale ordering of variables. The D-vine layout for five-dimensional drought is graphically depicted in Fig. 8a. Moreover, Fig. 8b suggests that more than three-quarters of training instances belong to D-vine. In sum, we can predetermine D-vine trees, which can reduce time complexity as the order of the nodes has been fixed. As a key step prior to determining the final standardized score, the Kendall function [setting (iv)] is implemented to convert the copula measure to the Kendall measure. In brief, the Kendall function is designed to describe the distribution functions of copula values in the whole measure space, as the same copula values are assumed to have the same impact. Figures 9a and 9b give geometrical interpretations of the copula measure and the Kendall measure. It can be seen that the copula measure represents the rectangular region starting from the origin, while the Kendall measure is depicted as the region bounded by the isolines of constant copula values. On the one hand, the theoretical significance of the Kendall measure is because the critical

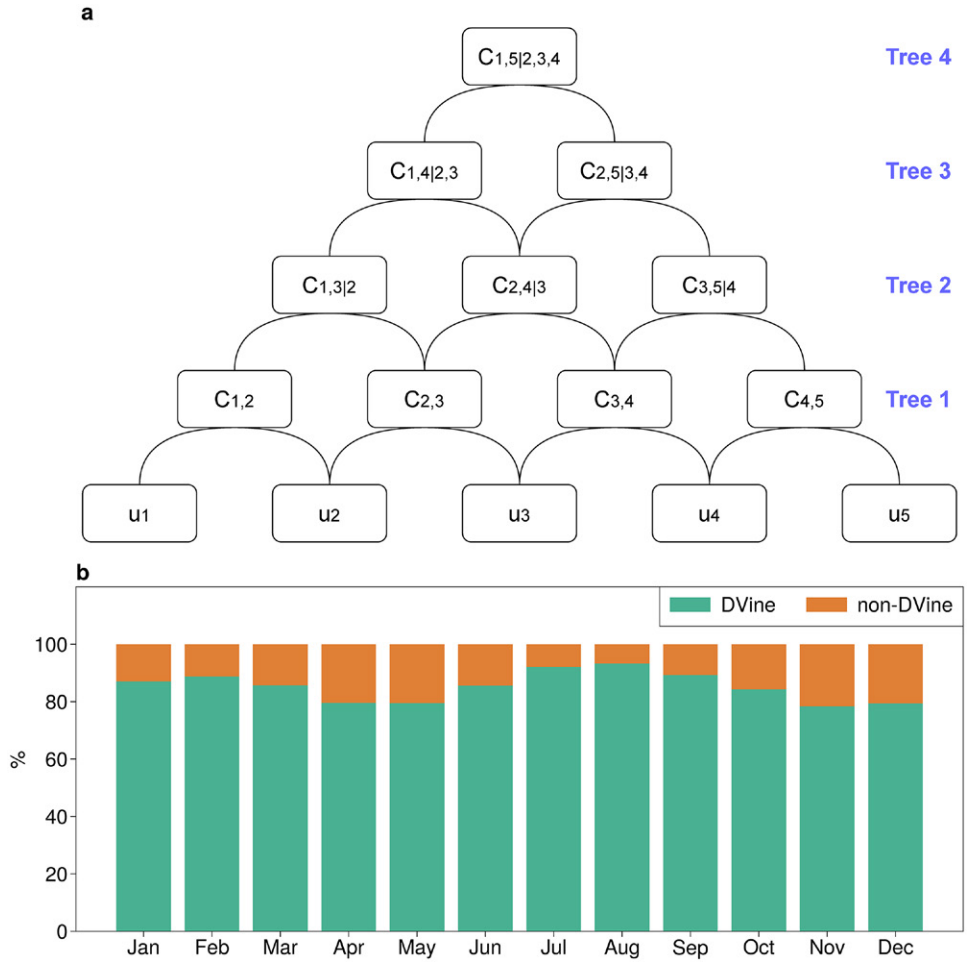

Fig. 8. (a) The structure of D-Vine in five dimensions. (b) The percentages of best-fit copulas falling in D-vine (green) and non-D-vine (orange) representation.

layer separating safe from dangerous events is unique for every design return period. More importantly in a practical sense, on the other hand, the Kendall measure is found to yield a complete symmetric index with a mean of zero, granting a fair chance of dry and wet events, as shown in the upper inset of Fig. 9b. In contrast, the indices created by copula measure contain a larger portion of negative than positive scores (upper inset of Fig. 9a), that is, 75%

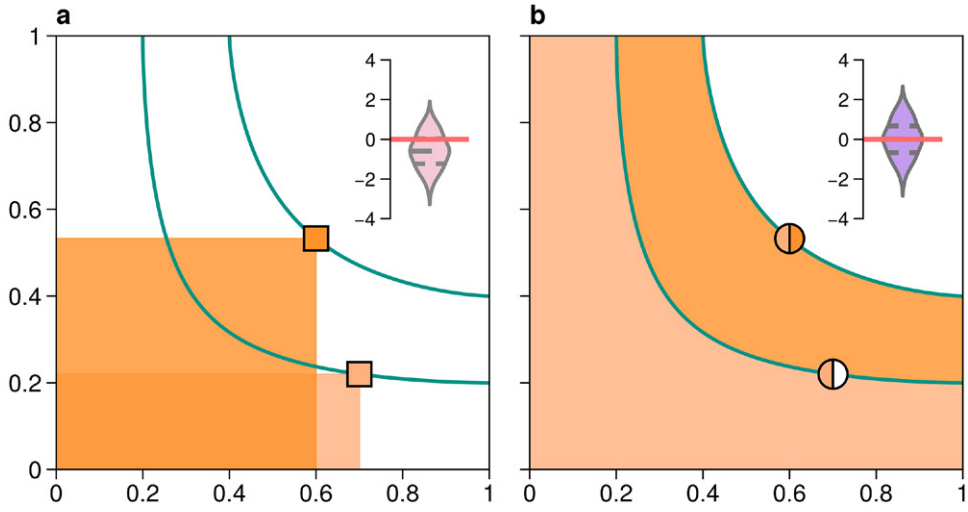

Fig. 9. Geometrical illustration of (a) copula measure and (b) Kendall measure, with the upper-right inset in each panel showing the frequency distribution of normalized scores expressed as a violin plot with the dashed horizontal lines representing the 25th, 50th, and 75th quantiles.

versus 25%. In short, we recommend using the Kendall measure to follow the general rule of drought index formulation.

The detailed descriptions pertaining to each specific setting are shown in section S4.3 in the supporting information.

Interpretation of CMI and super drought recognition

In this section, we demonstrate the properties of CMI and super drought recognition. Figure 10a affords a straightforward illustration of joining multiscalar dry–wet states based on CMI at May 2016. Further, we will assess again the three cases as marked in Fig. 1 to better demonstrate the powerful ability of CMI, as illustrated in Fig. 10b. In August 2018, the SPEI values at the five time scales are [−1.8, −2.1, −1.7, −1.6, −1.9], and the composite effect as denoted by the CMI value is −2.2, implying the emergence of super drought. At first glance, the result seems bewildering in its magnitude, as the maximum and mean magnitude of input

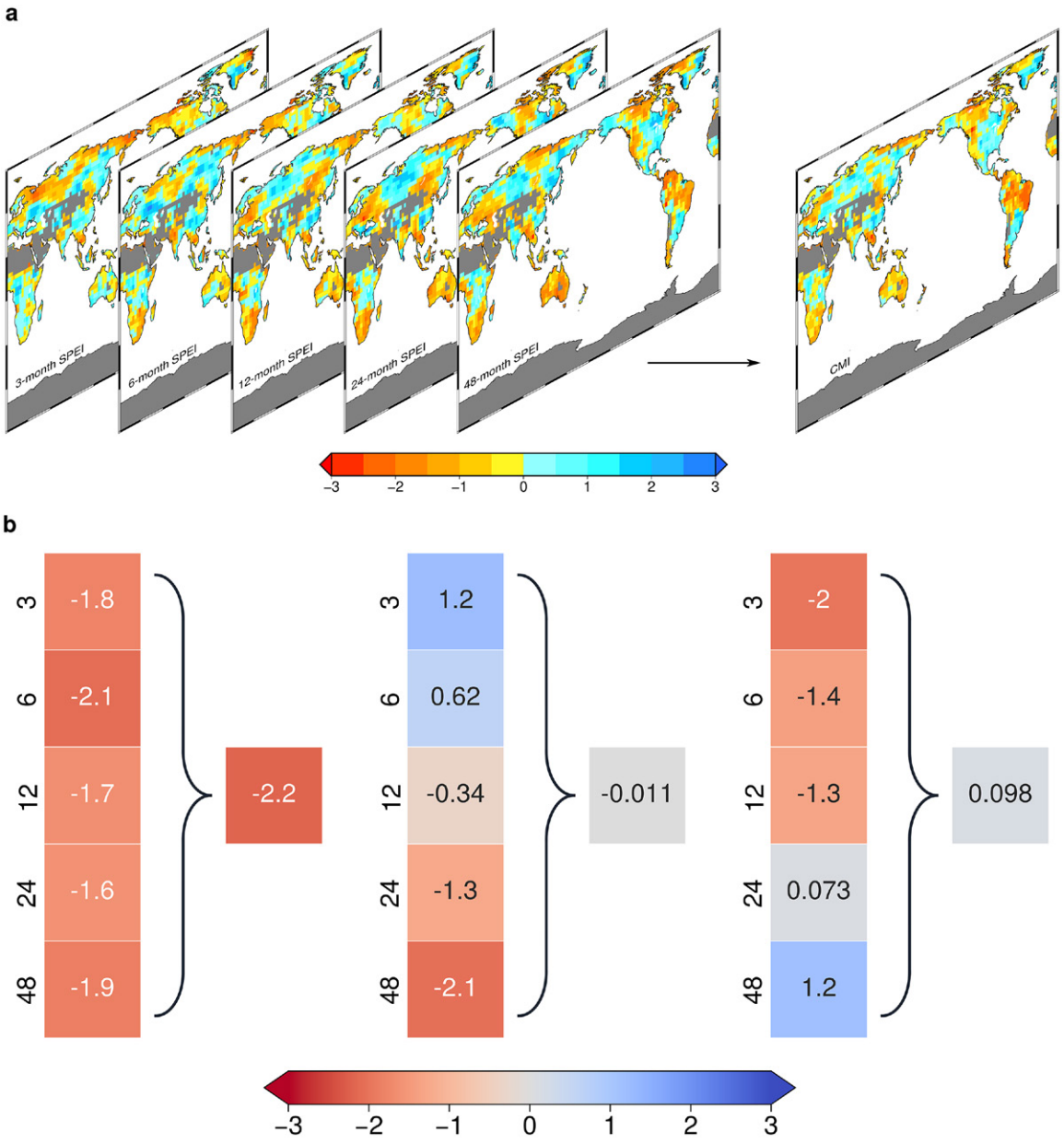

Fig. 10. Examples of joining multiscalar dry–wet states based on the proposed vine copula framework, in terms of spatial pattern on a globe in (a) May 2016 and (b) three representative samples. The three samples are collected in August 2018, October 2020, and November 1982 at the grid point 49.5°N, 13.5°E, which are marked in Fig. 1.

signals are −2.1 and −1.82 ([−1.8−2.1 − 1.7 − 1.6 − 1.9]/5 = −1.82), respectively. It has to be pointed out that the resultant value of −2.2 reflects the probability of drought combination risk under the whole measure space. In this way, the above result is expected as the joint likelihood of multidimensional drought peaks is even more rare. As a result, the coincidence probability must be extremely low and the joint score tends to be more negative than each component. The other two cases of October 2020 and November 1982 feature coexisting of dry and wet conditions. The resultant CMI is found to be near zero, representing overall normal condition. This is plausible because the positive and negative anomalies tend to cancel out.

In summary, the advantage of CMI is that it comprehensively explores the whole measure space and optimally determines how unusual the multidimensional observation is. In contrast, the linear combination perspective does not make use of the whole measure space and is thus not able to provide information accurately. As indicated by all above cases, the CMI value is significantly distinct from the mean value of the components. This affirms that the composite behavior is normally not a linear average of the individual behaviors.

Next, it is interesting to explore the relation between CMI and multiscalar SPEI when super drought occurs. Since multiscalar SPEI being high-dimensional is very hard to process, principal component analysis (PCA) is employed to reduce the dimensionality by extracting the most important feature. To guarantee the robustness, prefiltering process and method of PCA are applied to observations over all points on a globe rather than on an individual grid cell. The first two rows of Fig. 11 report the eigenvector and the frequency histogram of PC scores over the first principal axis. Each panel, from left to right, corresponds to the precondition CMI < −1.5, CMI < −2, and CMI < −2.5. These thresholds are referred to as CMI critical values. As indicated by the variance contribution, the first leading mode accounts for more than 90% of total variance, so the one-dimensional representation is a very good approximation to the original SPEIs in five-dimensional space. As shown by the eigenvector, it can be seen that all loadings have the same sign and similar magnitude, meaning in-phase variation pattern along the time-scale dimension. Owing to the overall coherent variability, we scale the eigenvector components to quasi-unit vector by a scaling factor and then multiply the PC score by the same factor. This rescaling does not alter the result, but has the strength of making the PC score be directly interpreted as the original SPEIs. Based on the histograms, we define the SPEI critical value that marks the 90th percentile.

With the above preparation, Fig. 11g illustrates the one-to-one relation between CMI critical values and SPEI critical values. For example, we see that CMI < −1.5 corresponds to SPEIs < −1.14, CMI < −2 to SPEIs < −1.57, and CMI < −2.5 to SPEIs < −1.64. Since the general rule is established through global-scale assessment, it is to a large extent appropriate in all situations and local significant exceptions to the rule would be in the minority. Figure 11g tells us two things. On the one hand, compared to SPEI critical values' profile, CMI critical values have a profile significantly shifted toward lower values. This shift again supports the view that simultaneous concurrence of extreme values can result in larger impact. On the other hand, there is a nonlinear interrelation between CMI and SPEI. When SPEIs become more negative, a small decrease in SPEIs leads to a large decrease in CMI. This means that adding extra pressure to individual drought type can cause the overall drought stress to deteriorate faster.

Validation of CMI

Aiming for integrated drought characterization and super drought detection, the validation of the proposed CMI is of vital importance. Ideally, the validating measurement should detect the same target as CMI, that is, stands out to capture drought features from an integrated perspective; meanwhile, global coverage is also required. Considering the above two aspects together, GRACE TWS available on a global scale is adopted as benchmark to test the worldwide skill of CMI and super drought identification. The reason is that up to now GRACE has had

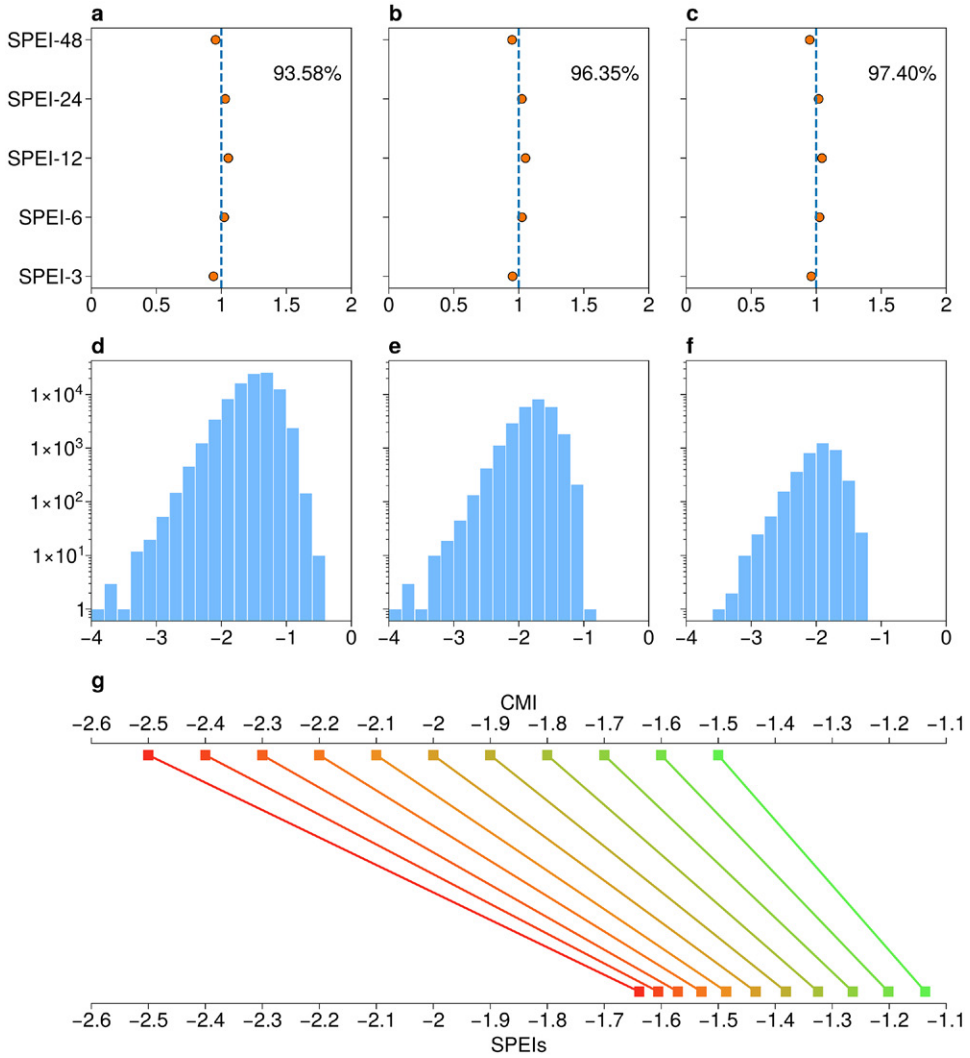

Fig. 11. (a)–(c) The eigenvectors and (d)–(f) the frequency histograms of PC scores over the first principal axis computed from SPEI at 3-, 6-, 12-, 24-, and 48-month time scales when CMI is less than (left) –1.5, (center) –2, and (right) –2.5. The explained variance of the first PC is labeled in the upper-right corner in (a)–(c). (g) Relation between CMI critical values and SPEI critical values, which are designated in the main text.

the unique ability to sense vertically integrated water storage and thus to comprehensively reflect changes in all of the available water (Deng et al. 2021), so that GRACE TWS is the only and best option for validating CMI. Nevertheless, this does not exclude the use of many other validating indicators (e.g., vegetation, soil moisture, actual records) in other specific aims. In this section, we conduct both a detailed case study and a global-scale assessment. In addition, a special focus is on investigating the ability of CMI to capture extreme events.

Case illustration. The central European drought (45°–50°N, 5°–20°E) in the summer of 2003 is used as a case study to demonstrate the merit of CMI as well as the significance of the super drought concept. Figure 12 portrays the dry–wet changes from the beginning of 2002 to the end of 2004 from multiple perspectives.

Figure 12b shows that central Europe experienced prolonged below-average rainfall from February to September 2003. When inspecting the conditions in March, the SPEI-3 is found to decrease to –1.68 and is accordingly allocated to the severe class (Fig. 12c), which was triggered by the consecutive precipitation deficit initiated in February. Similarly, most striking in Fig. 12a is that the 3-month water balance jumped from a low percentile score of 9.8% in January to an extremely high percentile score of 96.7% in March. However, Fig. 12a shows

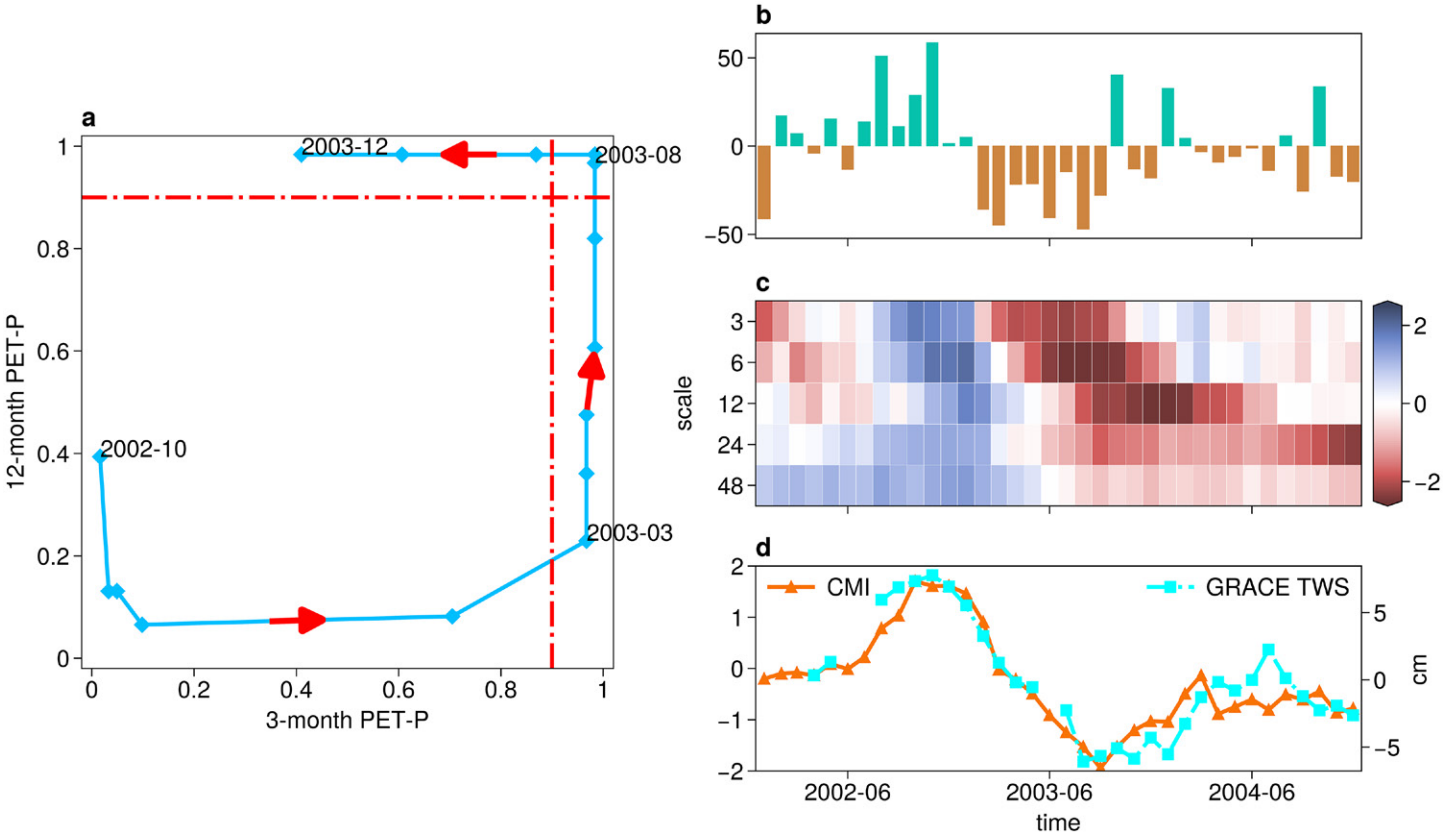

Fig. 12. (a) The track of dry–wet evolution from October 2002 to December 2003 depending upon the percentiles of 3-month (*x* axis) and 12-month (*y* axis) scale PET – P. Values around 0.5 are normal conditions, values above 0.5 indicate dry to exceptional drought conditions, and values below 0.5 represent wet to exceptional wet conditions. (b) Temporal evolution of precipitation anomalies, (c) SPEI at the time scales of 3, 6, 12, 24, and 48 months, and (d) CMI and GRACE TWS during January 2002–December 2004. The domain for the analysis is over central Europe (45°–50°N, 5°–20°E).

that the 12-month water balance exhibits a smoother temporal signal and remains on the lower end of the percentile score. Besides, considering time scales greater than 12 months, positive SPEI values between 0.26 and 0.95, indicative of humid conditions, are observed in March (Fig. 12c). This can be attributed to the fact that the long-term water balance has "memory" and the spring of 2003 was preceded by generous precipitation (Fig. 12b), which played a key role in suppressing long-term drought. As a consequence, it is no surprise to find TWS characterized by near-normal status (Fig. 12d). Meanwhile, the proposed CMI also has a value close to zero, confirming a good agreement with TWS. In conclusion, with the concept of super drought and CMI, it turns out no overall water deficits occurred in March 2003, despite the presence of short-term extreme drought.

From March 2003 onward, a continued series of short-term dry events (Fig. 12b) frequently hit central Europe, which is crucial to invoking long-term drought. As shown in Fig. 12c, negative SPEI values propagate from short to long scales with a time lag of several months. As March progressed to August and September, the 12-month water balance reached the highest percentile score of 0.98, falling in extremely dry conditions (Fig. 12a). Further, it can be seen in the top-right corner of Fig. 12a that the extreme phases of short-term and long-term drought coincided in August and September. In other words, concurrent extremes of drought at multiple time scales resulted in super drought, with CMI showing a minimum value equal to −1.94 as the lowest annual drought level (Fig. 12d). The presence of such a super drought event is corroborated by the measure of TWS, which declined to the concordant lowest value at −6 cm. In short, the essential feature behind the European drought in the late summer of 2003 is super drought.

After the summer of 2003, the long-term drought remained continuously in an extremely dry category (Fig. 12c). However, the super drought ended thanks to the recovery of short-term

drought in response to short-lived ample precipitation (Fig. 12b). As shown in Fig. 12a, the short-scale water balance returned to normal conditions toward the end of 2013, despite lingering hydrological drought. Thereby, no super drought showed up after the summer of 2003 due to the disappearance of drought overlap, preventing drought tensions from being far worse.

The above analysis has explained the formation mechanism of super drought by exploring the whole process of regional mean drought evolution. To gain deeper insights into what makes the intrinsic difference between high-impact droughts and those causing mild damage, the spatial comparison between the drought status of March and August 2003 is presented in Fig. 13. Notice that the original high resolution of 0.5° is adopted to facilitate spatial analysis at regional scale. In March 2003, it is apparent that substantial negative precipitation departures covered broad areas of the central Europe and short-term 3-month SPEI fell in the severe to extreme dry categories, which bears a great resemblance to the pattern in August 2003. However, why was devastating drought not perceived in March 2003? Neither precipitation anomalies nor traditional drought indices are able to explain this issue, owing to a lack of a comprehensive treatment of drought. By depending

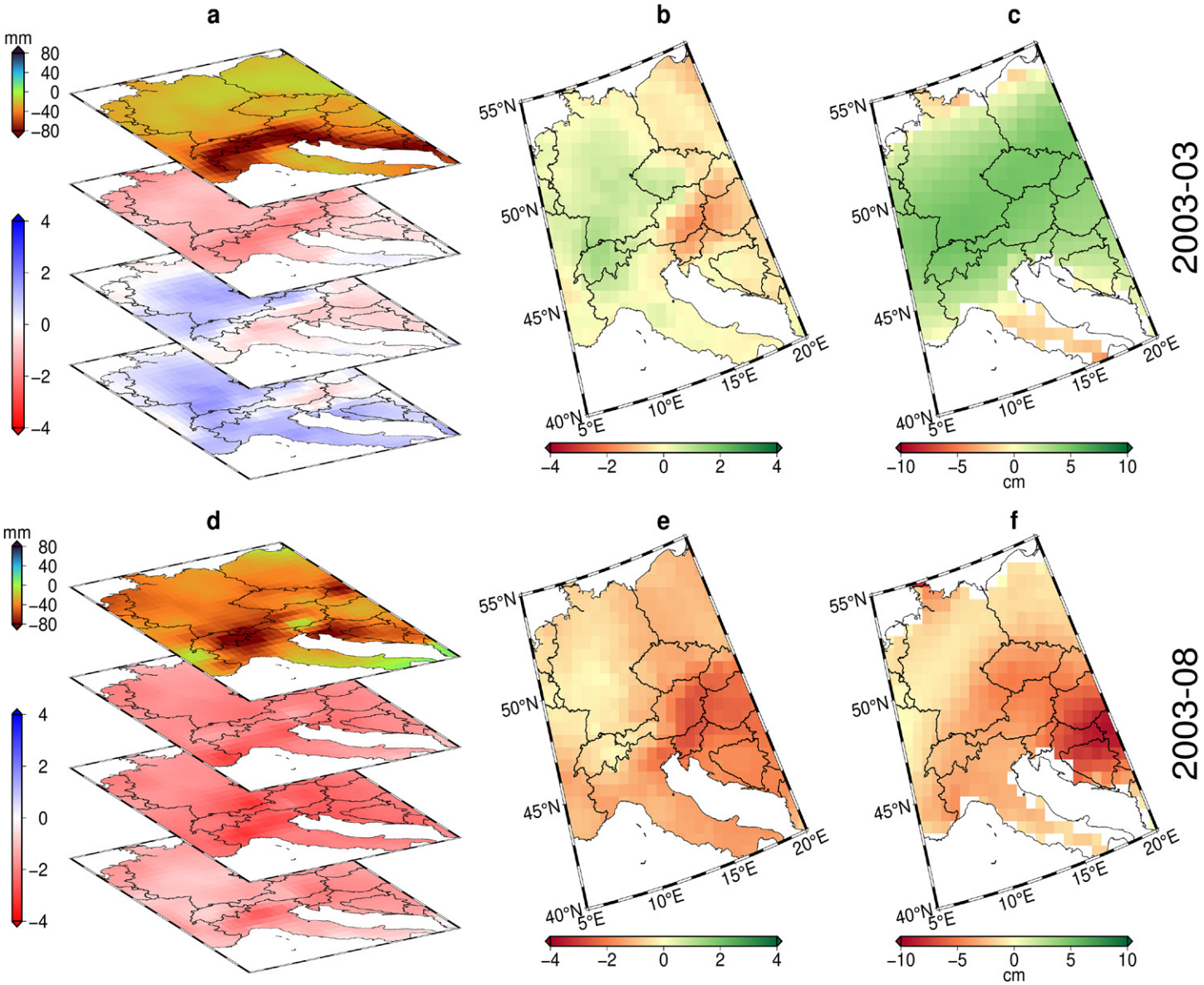

Fig. 13. Spatial comparison between the drought status of (a)–(c) March and (d)–(f) August 2003 over central Europe. The drought metrics analyzed are based on (a),(d) precipitation, SPEI-3, SPEI-6, and SPEI-12 (arranged in a stack from top to bottom), (b),(e) CMI, and (c),(f) GRACE TWS.

on the super drought concept and the CMI index developed, it can be easily interpreted as an absence of concurrent extremes at multiple time scales, because normal to wet conditions were noticed at medium to long time scales. As a consequence, it is not surprising to find CMI characterized by overall normal to wet conditions (Fig. 13b), which agrees well with the observed positive water thickness measured by GRACE (Fig. 13c). Therefore, the case in March 2003 suggests that individually occurring drought in a certain component leads to relatively moderate stress and that CMI successfully avoids false alarm, while traditional practices fail to achieve. Turning to the case in August 2003, it can be seen that extreme droughts at multiple time scales coincided (Fig. 13d), which is expected to yield more severe damage and widespread disruption to human society than events occurring in isolation. This is responsible for the substantial deficit of total water storage, as shown in Fig. 13f. Perfectly consistent with GRACE TWS observations, the CMI has good capability to reproduce the drought pattern with the most intense being located in the southeast sector (Fig. 13e). In sum, the comparison between the cases in March and August 2003 make it clear that the essential feature behind devastating drought is not that precipitation is deficient, soil moisture is drying out, or lake/reservoir water levels are depleted, but a combination of multiple drought extremes or equivalently grand loss in the total water storage.

The above case study illustrates the necessity and physical significance of the super drought concept, which is useful to improve the understanding of overall drought extremity. Meanwhile, the proposed CMI performs well to monitor super drought events as well as to exclude inconsequential ones and thus avoid false alarms.

Global-scale assessment. The global-scale performance of CMI in reproducing TWS is evaluated and compared against that of SPEI using correlation coefficient (CC), effective p value, and root-mean-square error (RMSE). The evaluation is made by a pixel-level comparison and boxplot summary of the skill scores computed globally, as depicted in Fig. 14.

First examined are the CC and associated p-value metrics, both of which describe the strength of the association. On the one hand, the correlation pattern (Fig. 14a) indicates a worldwide better ability of CMI than SPEI to capture TWS variability, with 0.1 higher CC on average. Particularly, the improvements in skill are more pronounced in the Eurasian continent, mainland Southeast Asian region, central-south North America, and Australia. On the other hand, the p-value pattern confirms the higher significance of the correlation between CMI and TWS, as reflected in Fig. 14c. Further, the boxplot (Fig. 14b) summarizing correlation coefficients indicates that although the correspondence between SPEI and TWS is good, the CMI offers higher skill. This is also true for the p-value score, because the median p value tested for CMI–TWS connection is 1.6×10^{-4}, about one order of magnitude smaller than that of SPEI. Most important, the annotations on top of the boxes highlight that the improvement in the simulation of TWS after applying CMI is statistically significant at the level of no less than 10^{-3}.

Next, the evaluation is further performed by calculating RMSE, which is relevant for evaluating the skill in reproducing the amplitude. Figure 14e clearly shows CMI generates fewer errors globally, with 58% of grid cells harboring RMSE of less than 1. The boxplot in Fig. 14f again proves that CMI causes the least deviation from TWS, as evidenced by the RMSE reduction ranging from 0.04 to 0.15 compared to SPEI. Meanwhile, the comparison of boxes supports that the capacity of CMI for reducing RMSE is statistically significant at 10^{-4} level.

In addition, in light of landmark role of self-calibrating PDSI (sc-PDSI) in the development of drought indices, section S6 in the supporting information compares the performance of CMI and sc-PDSI in estimating the overall drought condition. As a result, CMI exhibits a better fit with GRACE TWS measurement than sc-PDSI.

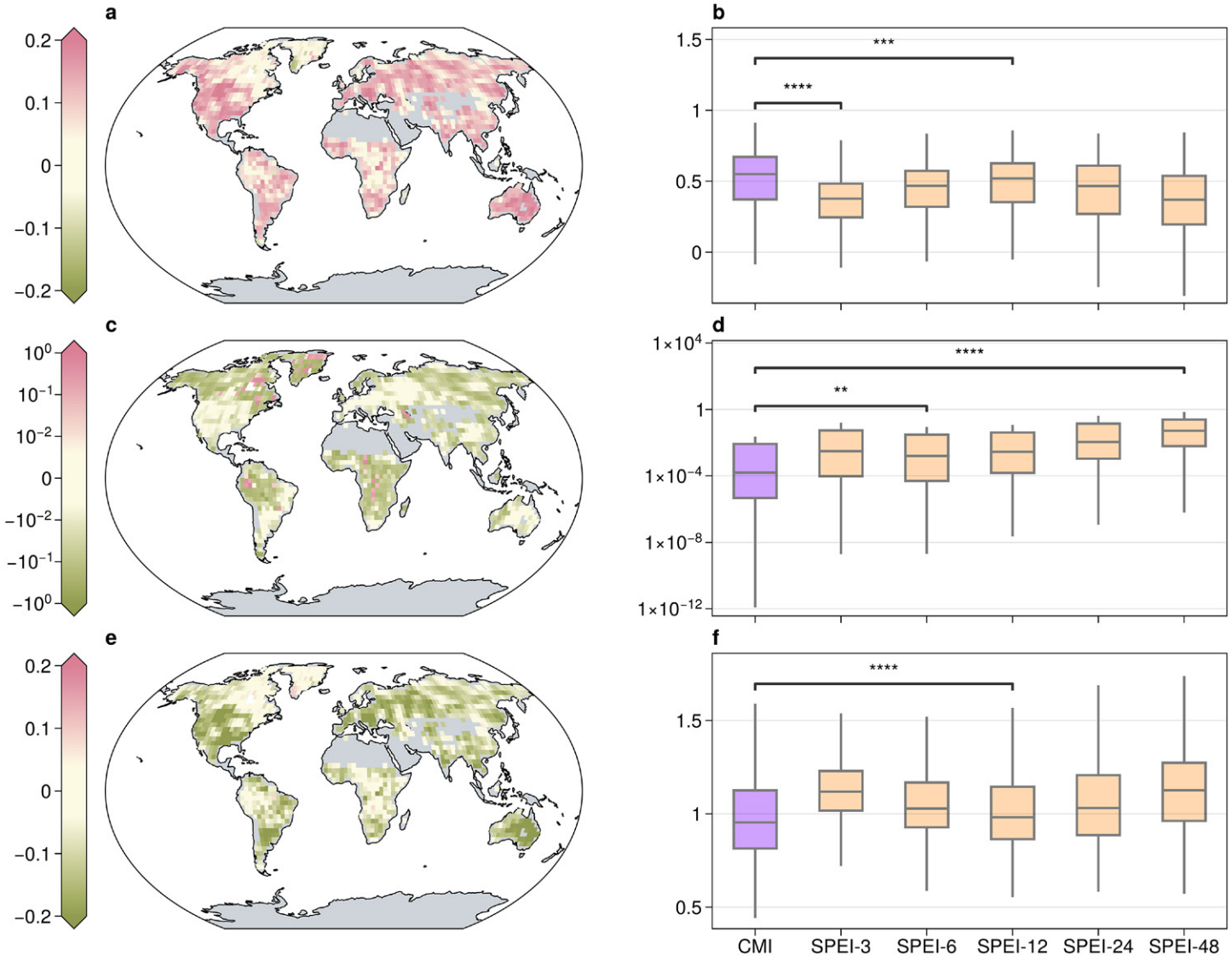

Fig. 14. (a),(c),(e) Spatial patterns of difference in skill metrics of CMI and SPEI against GRACE TWS. A symmetric logarithmic color scale is used for (c) with the scaling being linear between [-10^{-2}, 10^{-2}] and logarithmic otherwise. (b),(d),(f) Boxplot comparisons of the skill metrics for CMI and SPEI. The skills are measured by (a),(b) correlation coefficient, (c),(d) *p* value, and (e),(f) RMSE, with the higher value of correlation coefficient and the lower value of *p* value and RMSE referring to better performance. The boxplot includes median, the lower and upper quartiles, and the lower and upper fences (Q1 − 1.5 × IQR and Q3 + 1.5 × IQR, where Q1, Q3, and IQR denote the 25th percentile, 75th percentile, and interquartile range, respectively). In addition, the asterisks on top describe distributions with a statistically different mean based on one-tailed *T* test. Two (**), three (***), and four (****) asterisks mean that the CMI outperforms SPEI with significance levels of 10^{-2}, 10^{-3}, and 10^{-4}, respectively.

In conclusion, the overall water deficit–surplus represented by CMI has higher skill than that represented by SPEI. Of course, this is not meant to make a judgment on which index is intrinsically better. Instead, each index offers specific features and functionalities, and the suitability needs to be decided by the context. This research establishes the CMI metric as better for describing the overall extremity of multiscalar drought and recognizing super drought, while SPEI is most relevant for identifying characteristics of different drought types.

Extremity assessment. Subsequently, we also evaluate to what extent the CMI-based super drought detection exhibits better skill to represent extreme TWS events. To this end, histograms of TWS are compared between the two kinds of cases: the synchronous and asynchronous occurrences of drought at multiple time scales. The synchronous event is indeed super drought, defined as CMI < −2.14 approximately corresponding to SPEIs < −1.5, while

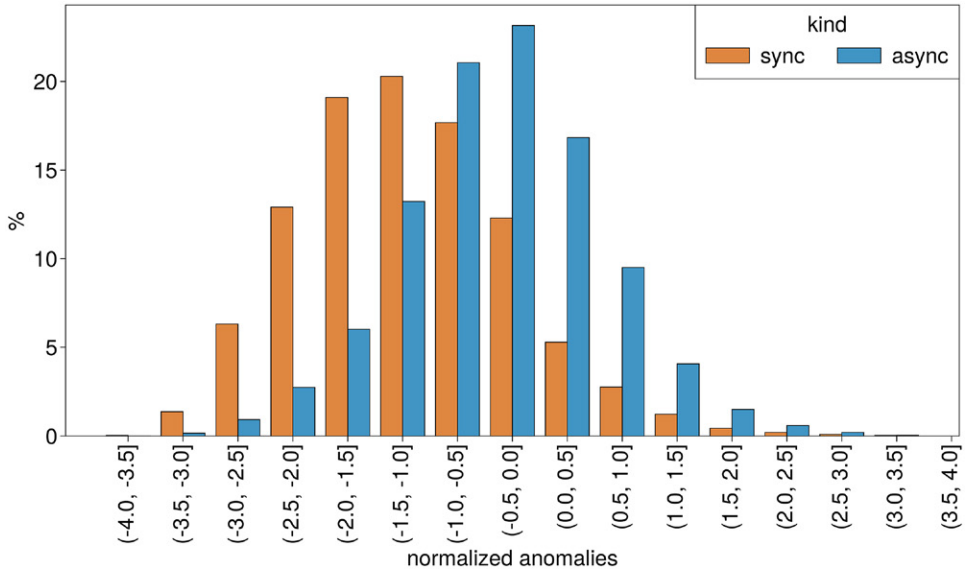

Fig. 15. A bin-to-bin comparison of frequency distribution (%) of normalized TWS anomalies between synchronous (orange bars) and asynchronous (blue bars) drought events. The definition for the synchronicity of drought events across multiple time scales can be found in the main text. Note that the synchronous event is indeed a super drought.

the asynchronous event is designated as severe drought (SPEI < −1.5) and humid status (SPEI > 0) coexisting. The result is visualized as a bin-to-bin histogram comparison of normalized TWS anomalies, as shown in Fig. 15.

The blue bars indicate that an asynchronous event yields a much weaker preference of positive or negative TWS and the percent contribution of TWS values less than one standard deviation is merely 23%. In the presence of super drought, in contrast, the frequency distribution of TWS is heavily skewed toward more negative values, with 90% and 60% of the values falling below 0 and −1 standard deviation, respectively.

In summary, the CMI-based super drought enables accurate estimation of the real water scarcity, which cannot be achieved by single time-scale fingerprint.

Discussion

In this section, we remark on some important issues, with detailed explanations reported in the supporting information.

Despite being driven by meteorological data, CMI does achieve the goal to quantitatively integrate multiple drought variables including agricultural and hydrological types. Furthermore, the proposed framework to calculate CMI is general enough to be used for various kinds of data sources other than meteorological data. The details are presented in section S5 of the supporting information. In addition, we have proven that the proposed CMI metric is not very sensitive to the influence of individual component behavior and does reflect the coexposure to multiple drought stresses. Refer to section S4.4 in the supporting information for details.

A special concern is that the proposed algorithm and parameter settings have been perceived as complex and numerically demanding. In section S4.5 of the supporting information, we highlight that the workflow is automated in merely three stages and has the outstanding advantage due to it being totally free from parameter settings. Meanwhile, the computing burden primarily exerted by the Monte Carlo simulation can be greatly alleviated by parallel programming.

Finally, it is noteworthy that the novel framework to calculate CMI does not consider asymmetry and nonstationarity in the modeling. The former one describes unequal impacts posed

by drought at different time scales. Section S4.6 in the supporting information suggests a feasible solution for how to incorporate asymmetric weights, which is inspired by portfolio value at risk theory (Byun and Song 2021). However, an absence of priori asymmetric information constitutes a major obstacle for application. The latter one is an important issue to be considered if the probable values for a certain period are typically outside the range of calibration in which the vine copula model is trained. However, the nonstationarity does not severely impact the validity of a vine copula fitting model in the historical 1961–2020 period (see section S4.7 in the supporting information for details). Moreover, (WMO (2012)) recommended that climatology length of 50–60 years is optimal and preferred to promote parameter stability in drought modeling. Although not currently accounted for, the nonstationarity must be coupled with future scenario projection, which is marked by a considerable degree of shifts in the underlying probability distribution. The basic idea to introduce nonstationarity is to express the fitting parameters as a function of time, which is usually called dynamic copula in financial science (Cherubini et al. 2012). We decide to develop the nonstationary version of CMI in the course of work evaluating the future scenario of super drought.

Conclusions

Monitoring and assessing extreme drought remain a profound challenge primarily owing to the multiscalar nature of drought. To overcome this challenge, the current study establishes the theoretical basis of the super drought concept, which refers to the simultaneous occurrence of extreme droughts at multiple time scales. The physical significance of super drought represents a combination of extreme dry states in multiple components of water resources or equivalently substantial deficits of total water storage, which is identified as the intrinsic difference compared to inconsequential ones with less impact. To have a quantitative representation, this study develops a complete framework based on vine copula and an associated novel monitoring index, CMI, in ways that are tailored to the needs of super drought detection. Furthermore, we interpret the properties of CMI and evaluate its performance against GRACE TWS at the global scale. The results demonstrate that CMI is a plausible metric to combine different forms of drought probabilistically and can better reflect overall rarity of water storage and recognize super drought.

The important issue to emphasize is that CMI is developed to describe the overall extremity of multiscalar drought and recognize super drought, but definitely it is not a universal solution that will be suitable for every specific application. Different drought indices offer specific features and functionalities. For this reason, CMI is not meant to replace other classic drought indices (WMO 2016). In addition to the novel concept and framework, accurate data sources are of equal importance to improve drought monitoring ability.

The current research is the first in a two-part series and constitutes a key prerequisite for advanced research and successful application. In the follow-up study, CMI will be used to explore super drought changes under global warming, including frequency–duration–area analysis, compilation of an event inventory, and driving mechanisms.

Finally, we create and manage a website (superdrought.com) to publish the CMI dataset and display near-real-time monitoring of global super drought. This web interface provides an operational assessment for overall drought risk, which not only benefits scientific end users for ease of use but decision-makers for drought preparedness and mitigation.

Acknowledgments. We thank the editor and the three anonymous referees for their valuable comments that helped to improve the manuscript. This work was supported by the National Natural Science Foundation of China Grants 42175041, 42230605, and 41831175, the International Partnership

Program of Chinese Academy of Sciences for Future Network (060GJHZ2022104FN), and the Second Tibetan Plateau Scientific Expedition and Research Program (2019QZKK0102).

Data availability statement. The CMI dataset generated in this study is available at superdrought.com. The CRU TS4.05 precipitation and PET data used to calculate CMI can be accessed online through https://data.ceda.ac.uk/badc/cru/data/cru_ts/cru_ts_4.05. The GRACE data used for validation can be downloaded from www2.csr.utexas.edu/grace/. The GlobCover land-cover data to exclude desert area can be downloaded from http://due.esrin.esa.int/page_globcover.php.

References

Aas, K., C. Czado, A. Frigessi, and H. Bakken, 2009: Pair-copula constructions of multiple dependence. *Insur. Math. Econ.*, **44**, 182–198, https://doi.org/10.1016/j.insmatheco.2007.02.001.

AghaKouchak, A., and Coauthors, 2021: Anthropogenic drought: Definition, challenges, and opportunities. *Rev. Geophys.*, **59**, e2019RG000683, https://doi.org/10.1029/2019RG000683.

Akaike, H., 1998: Information theory and an extension of the maximum likelihood principle. *Selected Papers of Hirotugu Akaike*, H. Akaike et al., Eds., Springer, 199–213.

Allen, R. G., M. Smith, L. S. Pereira, and A. Perrier, 1994: An update for the calculation of reference evapotranspiration. *ICID Bull.*, **43**, 35–92.

Ault, T. R., 2020: On the essentials of drought in a changing climate. *Science*, **368**, 256–260, https://doi.org/10.1126/science.aaz5492.

Bedford, T., and R. M. Cooke, 2002: Vines—A new graphical model for dependent random variables. *Ann. Stat.*, **30**, 1031–1068, https://doi.org/10.1214/aos/1031689016.

Beguería, S., S. M. Vicente-Serrano, and M. Angulo-Martínez, 2010: A multiscalar global drought dataset: The SPEIbase: A new gridded product for the analysis of drought variability and impacts. *Bull. Amer. Meteor. Soc.*, **91**, 1351–1356, https://doi.org/10.1175/2010BAMS2988.1.

Berg, A., and K. A. McColl, 2021: No projected global drylands expansion under greenhouse warming. *Nat. Climate Change*, **11**, 331–337, https://doi.org/10.1038/s41558-021-01007-8.

Byun, K., and S. Song, 2021: Value at risk of portfolios using copulas. *Commun. Stat. Appl. Methods*, **28**, 59–79, https://doi.org/10.29220/CSAM.2021.28.1.059.

Cherubini, U., F. Gobbi, S. Mulinacci, and S. Romagnoli, 2012: *Dynamic Copula Methods in Finance.* John Wiley and Sons, 288 pp.

Czado, C., 2019: *Analyzing Dependent Data with Vine Copulas: A Practical Guide with R.* Springer, 242 pp.

Dai, A., 2011: Drought under global warming: A review. *Wiley Interdiscip. Rev.: Climate Change*, **2**, 45–65, https://doi.org/10.1002/wcc.81.

——, 2013: Increasing drought under global warming in observations and models. *Nat. Climate Change*, **3**, 52–58, https://doi.org/10.1038/nclimate1633.

Deng, S., S. Liu, and X. Mo, 2021: Assessment and attribution of China's droughts using an integrated drought index derived from GRACE and GRACE-FO data. *J. Hydrol.*, **603**, 127170, https://doi.org/10.1016/j.jhydrol.2021.127170.

Fu, Q., and S. Feng, 2014: Responses of terrestrial aridity to global warming. *J. Geophys. Res. Atmos.*, **119**, 7863–7875, https://doi.org/10.1002/2014JD021608.

Guan, X. J., J. Ma, R. Huang, L. Huang, and Z. M. A. Zhang, 2019: Impact of oceans on climate change in drylands. *Sci. China Earth Sci.*, **62**, 891–908, https://doi.org/10.1007/s11430-018-9317-8.

Hao, Z., and A. AghaKouchak, 2013: Multivariate standardized drought index: A parametric multi-index model. *Adv. Water Resour.*, **57**, 12–18, https://doi.org/10.1016/j.advwatres.2013.03.009.

——, and V. P. Singh, 2015: Drought characterization from a multivariate perspective: A review. *J. Hydrol.*, **527**, 668–678, https://doi.org/10.1016/j.jhydrol.2015.05.031.

——, F. Hao, and V. P. Singh, 2016: A general framework for multivariate multi-index drought prediction based on multivariate ensemble streamflow prediction (MESP). *J. Hydrol.*, **539**, 1–10, https://doi.org/10.1016/j.jhydrol.2016.04.074.

Harris, I., T. J. Osborn, P. Jones, and D. Lister, 2020: Version 4 of the CRU TS monthly high-resolution gridded multivariate climate dataset. *Sci. Data*, **7**, 109, https://doi.org/10.1038/s41597-020-0453-3.

Hayes, M., M. Svoboda, N. Wall, and M. Widhalm, 2011: The Lincoln declaration on drought indices: Universal meteorological drought index recommended. *Bull. Amer. Meteor. Soc.*, **92**, 485–488, https://doi.org/10.1175/2010BAMS3103.1.

He, X., M. Pan, Z. Wei, E. F. Wood, and J. Sheffield, 2020: A global drought and flood catalogue from 1950 to 2016. *Bull. Amer. Meteor. Soc.*, **101**, E508–E535, https://doi.org/10.1175/BAMS-D-18-0269.1.

Hofert, M., I. Kojadinovic, M. Machler, and J. Yan, 2018: *Elements of Copula Modeling with R.* Springer International, 267 pp.

Huang, J., H. Yu, X. Guan, G. Wang, and R. Guo, 2016: Accelerated dryland expansion under climate change. *Nat. Climate Change*, **6**, 166–171, https://doi.org/10.1038/nclimate2837.

——, and Coauthors, 2017: Dryland climate change: Recent progress and challenges. *Rev. Geophys.*, **55**, 719–778, https://doi.org/10.1002/2016RG000550.

Joe, H., 1996: Families of m-variate distributions with given margins and $m(m-1)/2$ bivariate dependence parameters. *Distributions with Fixed Marginals and Related Topics, Lecture Notes Monogr.*, Vol. 28, Institute of Mathematical Statistics, 120–141.

Kao, S.-C., and R. S. Govindaraju, 2008: Trivariate statistical analysis of extreme rainfall events via the Plackett family of copulas. *Water Resour. Res.*, **44**, W02415, https://doi.org/10.1029/2007WR006261.

——, and ——, 2010: A copula-based joint deficit index for droughts. *J. Hydrol.*, **380**, 121–134, https://doi.org/10.1016/j.jhydrol.2009.10.029.

Keyantash, J. A., and J. A. Dracup, 2004: An aggregate drought index: Assessing drought severity based on fluctuations in the hydrologic cycle and surface water storage. *Water Resour. Res.*, **40**, W09304, https://doi.org/10.1029/2003WR002610.

Klein Tank, A. M. G., F. W. Zwiers, and X. Zhang, 2009: Guidelines on analysis of extremes in a changing climate in support of informed decisions for adaptation. WMO Rep. WMO/TD-1500, 56 pp., https://library.wmo.int/index.php?lvl=notice_display&id=138#.ZCrDBXZByUk.

Kurowicka, D., and H. Joe, Eds., 2011: *Dependence Modeling: Vine Copula Handbook.* World Scientific, 360 pp.

Landerer, F. W., and S. S. Cooley, 2021: GRACE D-103133 Gravity Recovery and Climate Experiment level-3 data product user handbook. NASA Jet Propulsion Laboratory Doc., 62 pp.

Lewis, S. L., P. M. Brando, O. L. Phillips, G. M. F. van der Heijden, and D. Nepstad, 2011: The 2010 Amazon drought. *Science*, **331**, 554, https://doi.org/10.1126/science.1200807.

Ma, M., L. Ren, V. P. Singh, X. Yang, F. Yuan, and S. Jiang, 2014: New variants of the Palmer drought scheme capable of integrated utility. *J. Hydrol.*, **519**, 1108–1119, https://doi.org/10.1016/j.jhydrol.2014.08.041.

——, ——, ——, X. Tu, S. Jiang, and Y. Liu, 2015: Evaluation and application of the SPDI-JDI for droughts in Texas, USA. *J. Hydrol.*, **521**, 34–45, https://doi.org/10.1016/j.jhydrol.2014.11.074.

McKee, T. B., N. J. Doesken, and J. Kleist, 1993: The relationship of drought frequency and duration to time scales. Preprints, *Eighth Conf. on Applied Climatology*, Anaheim, CA, Amer. Meteor. Soc., 179–184.

Mo, K. C., and D. P. Lettenmaier, 2014: Objective drought classification using multiple land surface models. *J. Hydrometeor.*, **15**, 990–1010, https://doi.org/10.1175/JHM-D-13-071.1.

Naumann, G., C. Cammalleri, L. Mentaschi, and L. Feyen, 2021: Increased economic drought impacts in Europe with anthropogenic warming. *Nat. Climate Change*, **11**, 485–491, https://doi.org/10.1038/s41558-021-01044-3.

Nelsen, R. B., 2007: *An Introduction to Copulas.* Springer Science and Business Media, 269 pp.

——, J. J. Quesada-Molina, J. A. Rodríguez-Lallena, and M. Úbeda-Flores, 2003: Kendall distribution functions. *Stat. Probab. Lett.*, **65**, 263–268, https://doi.org/10.1016/j.spl.2003.08.002.

Pascale, S., S. B. Kapnick, T. L. Delworth, and W. F. Cooke, 2020: Increasing risk of another Cape Town "day zero" drought in the 21st century. *Proc. Natl. Acad. Sci. USA*, **117**, 29 495–29 503, https://doi.org/10.1073/pnas.2009144117.

Peterson, T. J., M. Saft, M. C. Peel, and A. John, 2021: Watersheds may not recover from drought. *Science*, **372**, 745–749, https://doi.org/10.1126/science.abd5085.

Qi, Y., H. Yu, Q. Fu, Q. Chen, J. Ran, and Z. Yang, 2022: Future changes in drought frequency due to changes in the mean and shape of the PDSI probability

density function under RCP4.5 scenario. *Front. Earth Sci.*, **10**, 857885, https://doi.org/10.3389/feart.2022.857885.

Rajsekhar, D., V. P. Singh, and A. K. Mishra, 2015: Multivariate drought index: An information theory based approach for integrated drought assessment. *J. Hydrol.*, **526**, 164–182, https://doi.org/10.1016/j.jhydrol.2014.11.031.

Save, H., S. Bettadpur, and B. D. Tapley, 2016: High-resolution CSR GRACE RL05 mascons. *J. Geophys. Res. Solid Earth*, **121**, 7547–7569, https://doi.org/10.1002/2016JB013007.

Schepsmeier, U., 2015: Efficient information based goodness-of-fit tests for vine copula models with fixed margins: A comprehensive review. *J. Multivar. Anal.*, **138**, 34–52, https://doi.org/10.1016/j.jmva.2015.01.001.

Shah, D., and V. Mishra, 2020: Integrated drought index (IDI) for drought monitoring and assessment in India. *Water Resour. Res.*, **56**, e2019WR026284, https://doi.org/10.1029/2019WR026284.

Sheffield, J., E. F. Wood, and M. L. Roderick, 2012: Little change in global drought over the past 60 years. *Nature*, **491**, 435–438, https://doi.org/10.1038/nature11575.

Sherwood, S., and Q. Fu, 2014: Climate change. A drier future? *Science*, **343**, 737–739, https://doi.org/10.1126/science.1247620.

Sklar, A. 1959: Fonctions de répartition à n dimensions et leurs marges. *Publ. Inst. Stat. Univ. Paris*, **8**, 229–231.

Spinoni, J., and Coauthors, 2020: Future global meteorological drought hot spots: A study based on CORDEX data. *J. Climate*, **33**, 3635–3661, https://doi.org/10.1175/JCLI-D-19-0084.1.

Tapley, B. D., and Coauthors, 2019: Contributions of GRACE to understanding climate change. *Nat. Climate Change*, **9**, 358–369, https://doi.org/10.1038/s41558-019-0456-2.

Trenberth, K. E., A. Dai, G. van der Schrier, P. D. Jones, J. Barichivich, K. R. Briffa, and J. Sheffield, 2014: Global warming and changes in drought. *Nat. Climate Change*, **4**, 17–22, https://doi.org/10.1038/nclimate2067.

UNCCD, 2022: Drought in numbers 2022—Restoration for readiness and resilience. UNCCD Rep., 51 pp., https://reliefweb.int/report/world/drought-numbers-2022-restoration-readiness-and-resilience.

UNDRR, 2020: The human cost of disasters—An overview of the last 20 years 2000-2019. UNDRR Rep., 30 pp., www.undrr.org/publication/human-cost-disasters-overview-last-20-years-2000-2019#:~:text=In%20the%20period%202000%20to,over%20the%20previous%20twenty%20years.

Van Loon, A. F., and Coauthors, 2016: Drought in the Anthropocene. *Nat. Geosci.*, **9**, 89–91, https://doi.org/10.1038/ngeo2646.

Vicente-Serrano, S. M., S. Beguería, and J. I. López-Moreno, 2010: A multiscalar drought index sensitive to global warming: The standardized precipitation evapotranspiration index. *J. Climate*, **23**, 1696–1718, https://doi.org/10.1175/2009JCLI2909.1.

——, ——, and ——, 2011: Comment on "Characteristics and trends in various forms of the Palmer drought severity index (PDSI) during 1900–2008" by Aiguo Dai. *J. Geophys. Res.*, **116**, D19112, https://doi.org/10.1029/2011JD016410.

——, and Coauthors, 2012: Performance of drought indices for ecological, agricultural, and hydrological applications. *Earth Interact.*, **16**, https://doi.org/10.1175/2012EI000434.1.

Wang, J., Q. Zhang, L. Zhang, Y. Wang, P. Yue, Y. Hu, and P. Ye, 2022: The global pattern and development trends and directions on the drought monitoring research from 1983 to 2020 by using bibliometric analysis. *Bull. Amer. Meteor. Soc.*, **103**, E2081–E2107, https://doi.org/10.1175/BAMS-D-21-0324.1.

Wang, L., W. Chen, W. Zhou, and G. Huang, 2015: Drought in Southwest China: A review. *Atmos. Ocean. Sci. Lett.*, **8**, 339–344, https://doi.org/10.3878/AOSL20150043.

——, ——, ——, and ——, 2016: Understanding and detecting super-extreme droughts in Southwest China through an integrated approach and index. *Quart. J. Roy. Meteor. Soc.*, **142**, 529–535, https://doi.org/10.1002/qj.2593.

——, ——, Q. Fu, G. Huang, Q. Wang, C. Chotamonsak, and A. Limsakul, 2022: Super droughts over East Asia since 1960 under the impacts of global warming and decadal variability. *Int. J. Climatol.*, **42**, 4508–4521, https://doi.org/10.1002/joc.7483.

Wang, S., J. Huang, and X. Yuan, 2021: Attribution of 2019 extreme spring–early summer hot drought over Yunnan in Southwestern China [in "Explaining Extreme Events of 2019 from a Climate Perspective"]. *Bull. Amer. Meteor. Soc.*, **102** (1), S91–S96, https://doi.org/10.1175/BAMS-D-20-0121.1.

Waseem, M., M. Ajmal, and T.-W. Kim, 2015: Development of a new composite drought index for multivariate drought assessment. *J. Hydrol.*, **527**, 30–37, https://doi.org/10.1016/j.jhydrol.2015.04.044.

Williams, A. P., B. I. Cook, and J. E. Smerdon, 2022: Rapid intensification of the emerging southwestern North American megadrought in 2020–2021. *Nat. Climate Change*, **12**, 232–234, https://doi.org/10.1038/s41558-022-01290-z.

WMO, 2012: Standardized precipitation index user guide. WMO Doc. WMO-1090, 16 pp., https://library.wmo.int/index.php?lvl=notice_display&id=13682#.ZFD8b2BII2c.

——, 2016: Handbook of drought indicators and indices. WMO Doc. WMO-1173, 45 pp., https://community.wmo.int/en/bookstore/handbook-drought-indicators-and-indices.

Xia, Y., M. B. Ek, C. D. Peters-Lidard, D. Mocko, M. Svoboda, J. Sheffield, and E. F. Wood, 2014: Application of USDM statistics in NLDAS-2: Optimal blended NLDAS drought index over the continental United States. *J. Geophys. Res. Atmos.*, **119**, 2947–2965, https://doi.org/10.1002/2013JD020994.

Yang, J., J. Chang, Y. Wang, Y. Li, H. Hu, Y. Chen, Q. Huang, and J. Yao, 2018: Comprehensive drought characteristics analysis based on a nonlinear multivariate drought index. *J. Hydrol.*, **557**, 651–667, https://doi.org/10.1016/j.jhydrol.2017.12.055.

Zhang, C., H. Liu, Y. Song, Y. Liao, J. Duan, W. Cai, and S. Wang, 2017: *Grades of Meteorological Drought.* China Quality Inspection Press, 24 pp.

Zhang, L., T. Zhou, X. Chen, P. Wu, N. Christidis, and F. C. Lott, 2020: The late spring drought of 2018 in South China [in "Explaining Extreme Events of 2018 from a Climate Perspective"]. *Bull. Amer. Meteor. Soc.*, **101** (1), S59–S64, https://doi.org/10.1175/BAMS-D-19-0202.1.

Zhao, T., and A. Dai, 2017: Uncertainties in historical changes and future projections of drought. Part II: Model-simulated historical and future drought changes. *Climatic Change*, **144**, 535–548, https://doi.org/10.1007/s10584-016-1742-x.

——, and ——, 2022: CMIP6 model-projected hydroclimatic and drought changes and their causes in the twenty-first century. *J. Climate*, **35**, 897–921, https://doi.org/10.1175/JCLI-D-21-0442.1.